Nanomechanics of Organic Layers and Biomenbranes

Gerard Oncins Marco

Universitat de Barcelona

Facultat de Química

Departament de Química Física

NANOMECHANICS OF ORGANIC LAYERS AND BIOMEMBRANES

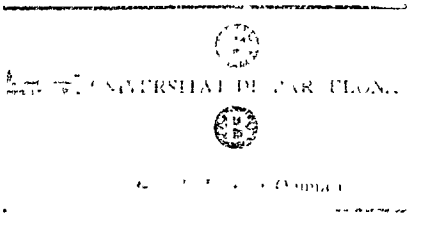

Gerard Oncins Marco

TESI DOCTORAL

3988 Langmuir 2006, 22, 3988−3998

Nanotribological Properties of Alkanephosphonic Acid Self-Assembled Monolayers on Aluminum Oxide: Effects of Fluorination and Substrate Crystallinity

Matthew J. Brukman,†‡ Gerard Oncins Marco,§ Timothy D. Dunbar,# Larry D. Boardman,# and Robert W. Carpick*†

Department of Engineering Physics, University of Wisconsin, Madison, Wisconsin 53706, Department of Physical Chemistry, University of Barcelona, Barcelona Spain, and 3M Corporate Research Materials Laboratory, St Paul, Minnesota 55144

Received October 22, 2005 In Final Form January 12, 2006

Two phosphonic acid (PA) self-assembled monolayers (SAMs) are studied on three aluminum oxide surfaces: the C and R crystallographic planes of single crystal α-alumina (sapphire) and an amorphous vapor-deposited alumina thin film. SAMs are either fully hydrogenated $CH_3(CH_2)_{17}PO_3H_2$ or semifluorinated $CF_3(CF_2)_7(CH_2)_{11}PO_3H_2$. Atomic force microscope (AFM) topographic imaging reveals that the deposited films are homogeneous, atomically smooth, and stable for months in the laboratory environment. Static and advancing contact angle measurements agree with previous work on identical or similar films, but receding measurements suggest reduced coverage here. To enable reproducible nanotribology measurements with the AFM, a scanning protocol is developed that leads to a stable configuration of the silicon tip. Adhesion for the semifluorinated films is either comparable to or lower than that for the hydrogenated films, with a dependence on contact history observed. Friction between each film and the tips depends strongly upon the type of molecule, with the fluorinated species exhibiting substantially higher friction. Subtle but reproducible differences in friction are observed for a given SAM depending on the substrate, revealing differences in packing density for the SAMs on the different substrates. Friction is seen to increase linearly with load, a consequence of the tip's penetration into the monolayer.

Introduction

Self-assembled monolayers (SAMs) have aroused great interest as a means of tailoring surfaces for micro- and nanoscale applications including biosensing,[1] stiction reduction,[2] micro- and nanolithography,[3] and corrosion resistance.[4] The most widely researched SAM precursor is the alkanethiol,[5] which is effective in reducing adhesion and friction on noble metals, particularly gold, but substrates for high-quality alkanethiol self-assembly are largely limited to these noble metals. Even on gold, the sulfur headgroup atom that binds it to the substrate will oxidize with time, leading to degradation of the corresponding tribological properties[6] in the absence of replenishing vapor- or liquid-phase molecules. Because strategies for nanotechnology typically include silicon lithography processes and new techniques that use other novel materials, it is critical to develop stable SAMs suitable for a wide range of native metal and semiconductor oxides. Two such materials are phosphonic acid (PA) and silane SAMs. The latter presents certain challenges in its deposition and surface attachment.[7,8] PA SAMs, however, form robust attachments to most metal oxides and are thus excellent candidates for a wide array of substrates.[9]

The alkanephosphonic acid molecule $CH_3(CH_2)_nPO_3H_2$ is a linear hydrocarbon chain with a phosphonic acid headgroup (P tetrahedrally bonded to C, O, and two OH groups) at the terminus. The headgroup is expected to bind to an oxide surface via two or three condensate bonds to surface oxygen atoms. Two species of alkanephosphonic acid are used in this investigation—one with a true alkane chain, $CH_3(CH_2)_{17}PO_3H_2$ (denoted $H_{18}PA$), and one fluorinated at the tail end, $CF_3(CF_2)_7(CH_2)_{11}PO_3H_2$ ($F_8H_{11}PA$). In a recent study, the identical semifluorinated molecule and fully alkane versions with either 16- or 22-carbon atoms were shown to form well-ordered monolayers on the native oxide of Al.[10]

Previous experimental and molecular dynamics studies have shown that other SAMs with terminal fluorine groups have surface properties distinct from those of fully hydrogenated SAMs.[11,12] Fluorinated SAMs are more hydrophobic and are superior electrical barriers compared to hydrogenated monolayers.[13] However, the nanoscale frictional forces measured against these surfaces are also significantly higher.[14,15] The fluorinated portion of a SAM molecule like $F_8H_{11}PA$ is also structurally different from that of an alkane chain. In the latter, the carbon backbone defines a single plane in the trans configuration. In $(CF_2)_n$ chains, however, the carbon atoms form a helix. Replacing H with F also

* Corresponding author E-mail: carpick@engr.wisc.edu Fax: +1 608-263-7451
§ University of Barcelona
# 3M Corporate Research Materials Laboratory
† University of Wisconsin
‡ Currently at North Carolina State University, Department of Physics

(1) Chaki, N. K.; Vijayamohanan, K. *Biosens. Bioelectron.* **2002**, *17*, 1−12.
(2) Ashurst, W. R.; Yau, C.; Carraro, C.; Lee, C.; Kluth, G. J.; Howe, R. T.; Maboudian, R. *Sens. Actuators, A* **2001**, *91*, 239−248.
(3) Friebel, S.; Aizenberg, J.; Abad, S.; Wiltzius, P. *Appl. Phys. Lett.* **2000**, *77*, 2406−2408.
(4) Whelan, C. M.; Kinsella, M.; Carbonell, L.; Ho, H. M.; Maex, K. *Microelectron. Eng.* **2003**, *70*, 551−557.
(5) Nuzzo, R. G.; Allara, D. L. *J. Am. Chem. Soc.* **1983**, *105*, 4481−4483.
(6) Kiely, J. D.; Houston, J. E. *Langmuir* **1999**, *15*, 4513−4519.
(7) Tegrange, J. D.; Markham, J. L.; Kurkjian, C. R. *Langmuir* **1993**, *9*, 1749−1753.
(8) Stevens, M. J. *Langmuir* **1999**, *15*, 2773−2778.
(9) van Alsten, J. G. *Langmuir* **1999**, *15*, 7605−7614.
(10) Pellerite, M. J.; Dunbar, T. D.; Boardman, L. D.; Wood, E. J. *J. Phys. Chem. B* **2003**, *107*, 11726−11736.
(11) Gao, J. P.; Luedtke, W. D.; Gourdon, D.; Ruths, M.; Israelachvili, J. N.; Landman, U. *J. Phys. Chem. B* **2004**, *108*, 3410−3425.
(12) Briscoe, B.; Evans, D. *Proc. R. Soc. London, Ser. A* **1982**, *380*, 389−407.
(13) Chidsey, C. E. D.; Loiacono, D. N. *Langmuir* **1990**, *6*, 682−691.
(14) Kim, H. I.; Koini, T.; Lee, T. R.; Perry, S. S. *Langmuir* **1997**, *13*, 7192−7196.
(15) DePalma, V.; Tillman, N. *Langmuir* **1989**, *5*, 868.

10.1021/la052847k CCC: $33.50
Published on Web 03/23/2006

increases the size of the individual molecules. Fluorinated chain segments have a van der Waals radius of 0.567 nm,[16] whereas the corresponding value for alkyl segments is 0.424 nm.[17] Structural differences between CH_2 and CF_2 chains make the latter stiffer, increasing the elastic modulus.[18-22] The mechanism(s) by which fluorinated SAMs exhibit greater shear strength (or friction) is not yet understood; candidate phenomena include packing[23] and changes in characteristic activation volumes,[12] while adhesion effects have been ruled out.[24]

The commercial availability of synthetic single crystal α-alumina (sapphire) with flat, oriented crystal faces, and the ease of depositing smooth films of amorphous alumina allow for a straightforward investigation of the dependence of monolayer quality on substrate surface crystallinity. The question of surface crystallinity occurs on two levels: First, either the surface is amorphous or crystalline. Then, if it is crystalline, the differences between crystallographic planes can be examined. The (1000) and (1$\bar{1}$02) planes, also known respectively as the C and R planes,[25-27] are used here in addition to an amorphous aluminum oxide thin film. The C-plane surface consists of hexagonally spaced oxygen atoms, packed three per unit mesh, which is a rhombus of area 0.196 nm^2. The R-plane unit mesh is rectangular and occupies 0.244 nm^2. In this mesh, two oxygen atoms lie on the surface with two more lying slightly lower but still exposed. These are shown in Figure 1 (adapted from Guo et al.[25]). The vapor-deposited alumina is expected to be amorphous without any long-range ordering of oxygen atoms.

Experimental Section

Substrates to be coated with SAMs were prepared as follows. Single crystal C- and R-plane sapphire crystals (MarkeTech International, Port Townsend, WA) were cleaned with piranha solution (4:1 H_2SO_4:H_2O_2 30% in H_2O) then annealed at 1300 °C for 48 h, then rinsed with ethanol. Piranha tends to leave oxide surfaces clean of hydrocarbons and well hydroxylated. It is very reactive with organic materials and should be used with great care. Alumina-coated (150 nm) Si (100) wafers (Silicon Valley Microelectronics, San Jose, CA) were rinsed with heptane, acetone, and 2-propanol, blown dry with N_2, and exposed to ultraviolet light (ozone cleaning) for 10 min. The amorphous and crystalline substrates were then immersed in 1 mM $F_8H_{11}PA$ or $H_{18}PA$ ethanol solutions for 24 h and rinsed with ethanol. Uncoated (blank) C- and R-plane sapphire dies were also piranha cleaned and ethanol rinsed and then annealed at 1300 °C shortly before initial AFM imaging. All samples were rinsed with ethanol again immediately before their initial imaging in the AFM.

Contact angles measurements with water and hexadecane were performed with an AST Products (Billerica, MA) VCA-2500XE video contact angle measurement apparatus. Drop volumes were 5 *μ*L for static and 3−7 *μ*L for the dynamic angle measurements in which fluid was added (advancing) or removed (receding) from the droplet. Reported here are average contact angles for at least two different samples of the same type. Hexadecane static measurements were indistinguishably close to advancing values and are not reported. Uncertainties in the contact angles are estimated to be ±2° for static and advancing angle measurements and ±5° for receding angle measurements. After contact angle measurements, all samples were washed with heptane and 2-propanol and blown dry with N_2.

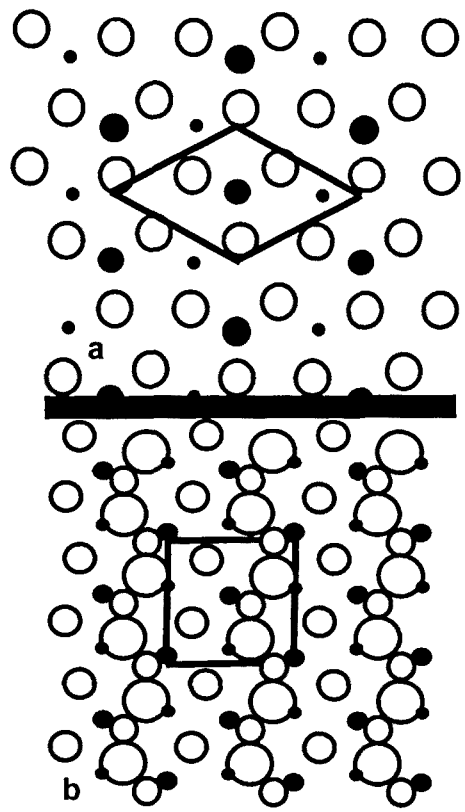

Figure 1. C plane (a) and R plane (b) surfaces, adapted from Ref. 25. Repeating mesh units are indicated by solid lines, oxygen by open circles, and aluminum by solid circles. Increased size indicates proximity to the surface.

Atomic force microscopy was performed with a Digital Instruments Multimode AFM with a Nanoscope IV controller. The instrument was placed on a vibration isolation platform and under a foam sound-absorbing hood in the ambient atmosphere with the temperature consistently 20−22 °C. The relative humidity varied from day to day, but preliminary work has shown that varying the humidity from 5 to 60% does not have a noticeable effect on friction or adhesion for these PA SAMs. The surfaces of both monolayers are hydrophobic, so water should not be strongly adsorbed to the surface at low to moderate ambient humidity.

Cantilevers were rectangular Si with its native oxide (Mikromasch, nominal dimensions 35 *μ*m × 300 *μ*m, nominal spring constant 0.2 N/m). Each lever's normal force constant was calibrated experimentally by Sader's unloaded resonance method,[28] with the plan view dimensions measured with the eyepiece of a Beuhler Micromet microindenter (Lake Bluff, IL). The lateral force calibration for

(16) Brandrup, J., Immergut, E. H. *Polymer Handbook*, 2nd ed., Wiley: New York, 1975.
(17) Tamada, K., Nagasawa, J., Nakanishi, F., Abe, K., Hara, M., Knoll, W., Ishida, T., Fukushima, H., Miyashita, S., Usui, T., Koini, T., Lee, T. R. *Thin Solid Films* **1998**, *329*, 150−155.
(18) Gallahet, K. L., Yokozeki, A., Bauer, S. H. *J. Phys. Chem.* **1974**, *78*, 2389−2395.
(19) Wolf, S. G., Deutsch, M., Landau, E. M., Lahav, M., Leiserowitz, L., Kjaer, K., Alsnielsen, J. *Science* **1988**, *242*, 1286−1290.
(20) Naselli, C., Swalen, J. D., Rabolt, J. F. *J. Chem. Phys.* **1989**, *90*, 3855−3860.
(21) Eaton, D. F., Smart, B. E. *J. Am. Chem. Soc.* **1990**, *112*, 2821−2823.
(22) Barton, S. W., Goudot, A., Bouloussa, O., Rondelez, F., Lin, B. H., Novak, F., Acero, A., Rice, S. A. *J. Chem. Phys.* **1992**, *96*, 1343−1351.
(23) Overney, R. M., Meyer, E., Frommer, J., Brodbeck, D., Luthi, R., Howald, L., Guntherodt, H.-J., Fujihara, M., Takano, H., Gotoh, Y. *Nature* **1992**, *359* (6391), 133.
(24) Chaudhury, M. K., Owen, M. J. *Langmuir* **1993**, *9*, 29−31.
(25) Guo, J., Ellis, D. Lam, D. *Phys. Rev. B* **1992**, *45*, 13647−13656.
(26) Hongo, H., Yudasaka, M., Ichihashi, T., Nihey, F., Iijima, S. Chemical vapor deposition of single-wall carbon nanotubes on iron-film-coated sapphire substrates. *Chem. Phys. Lett.* **2002**, *361*, 349−354.
(27) Guo, J., Ellis, D. E., Lam, D. J. *Phys. Rev. B* **1992**, *45*, 3204−3214.
(28) Sader, J., Chon, J., Mulvaney, P. *Rev. Sci. Instrum.* **1999**, *70*, 3967−3969.

each cantilever measured via the wedge method [29,30] was performed using a calibration grating (Mikromasch TGG01) providing two facets oriented at a known dihedral angle. Open-source Matlab scripts [31] were used to extract and average the optical sensitivity (photodetector signal volts/nm of cantilever motion) from batches of force−distance curves and to generate the data plots required for the calibration calculations. The scripts were also used to generate individual force-calibrated friction-load data sets from the raw Nanoscope output files.

For friction versus load (FL) studies, a slowly descending sawtooth waveform from an external function generator was added to the setpoint signal (at the Quadrex board of the Nanoscope IV controller), allowing the feedback control to continuously decrease the normal force over the course of an image. The FL images were 25 nm scans (perpendicular to the long axis of the cantilever) acquired at 6.1 Hz, with 512 lines and 512 pixels per line, corresponding to a scan velocity of 152.5 nm/s. Although the slow scan axis was turned off, there was still considerable tip motion longitudinally (along the surface parallel to the long axis of the cantilever) due to the intrinsic geometric coupling between the vertical and longitudinal displacement of the tip relative to the sample created by the tilt angle of the cantilever.[7,32] Depending on the load range for a given FL measurement, this total longitudinal tip displacement was never more than 200 nm. As discussed below, the samples were sufficiently homogeneous that this had no effect on the measurements. Imaging the selected region before and after the measurements ensured that step edges and any other defects were avoided during FL measurements.

Initially, the frictional force between the tip and sample changed as measurements were repeated under otherwise identical conditions. This could be explained only by the transfer of molecules from the SAM to the tip, a phenomenon that has been observed previously for silane films.[4] This necessitated a run-in procedure to stabilize the tip. A steady-state tip surface was attained by scanning the tip against the SAM at appreciable loads (50 to 100 nN) on the sample before performing FL measurements. New regions of the sample were always used for measurements after the tip treatment procedure was carried out. This is similar to a previously reported method of tip treatment[4] by scanning the tip against a mica sample, except that here the sample used for treatment and measurement is the same. A comprehensive discussion of the tip treatment process, including a demonstration of the tip contamination that it remedies, is presented in the Results section.

Friction forces were determined in the standard manner by taking the half-width of the trace−retrace friction loops for each fast-scan line of the image, averaged over the center 256 pixels of each 512-pixel line to avoid the sticking portion of the loop. The normal load signal was similarly averaged. Because the setpoint was varied continuously, the corresponding uncertainty associated with the normal force for each point in a given FL experiment is 1/1700th of the total range of the peak-to-peak force for that trace. Ten to 20 friction-load images were taken per sample, 5 to 10 at one location and an equal number at another location a few hundred nanometers away. Averages of the friction-load measurements were determined by combining data sets from a given location, sorting by the normal force, and averaging the normal and frictional forces in groups of consistent ranges of normal force. The 95% confidence intervals within the groups of 10 were generally less than 0.1 nN in normal force and <10% of the average lateral force for each group.

Except at loads just greater than the pull-off load, individual friction-load measurements were essentially linear. This is in contrast to the numerous observations of nonlinear friction-load behavior for solid−solid interfaces.[5,6] This has been attributed to a direct dependence of friction upon the contact area, which varies with load in a nonlinear fashion because of elastic deformation. Without further information about the contact area, we are unable to connect the interfacial shear strength (frictional force per unit area) directly to the frictional force, although the linear dependence is suggestive of either a linear pressure dependence of the shear strength[11,17] or the fact that the frictional force is not primarily related to the interfacial contact area. This will be revisited in the Discussion section. A useful metric for comparing the frictional properties of the surfaces is the slope of the FL traces, which we denote as α, having the physical interpretation of the average differential friction for a given FL measurement or "single-asperity friction coefficient."

Another metric of interest is the pull-off force between the tip and sample. This was determined both from force−distance (FD) curves, in which the sample is raised into contact with the tip and then withdrawn, and from the FL measurements previously described. In both types of measurement, the pull-off force was taken to be the difference in normal force between the unloaded out-of-contact position and the last data point acquired before the tip pulls out of contact with the sample. FD and FL measurement procedures are different in that FDs are much shorter in duration (total time per measurement: 0.5 versus 85 s) and involve less sliding because the tip is not being scanned laterally during the measurement.

Several cantilevers were used in these experiments to establish reproducibility. The tip of each lever was imaged by shadow transmission electron microscopy before use in the AFM to ensure that the tip shape was well defined and smoothly curved and had a small radius of curvature. Initially having radii of curvature of 20 nm or less, they were worn to radii of up to 47 nm [7] over the course of the hours of sliding contact involved in a given experiment. This effect was anticipated and was accounted for by cycling through all of the samples twice in a given experiment. Thus, the first measurements could be compared to those taken on the same sample hours later. Whereas pull-off forces tended to increase with tip use, the friction measurements, particularly the slopes of the FL plots, were very consistent for a given sample and are used as the figures of merit in quantifying friction. Although the meaning of the slope will be explained in the Discussion section, it is worth emphasizing here that the slopes α were not affected by these changes in tip radius.

Each sample was imaged topographically before friction measurements were performed. Both SAM-coated C-plane and blank C-plane sapphire substrates had wide terraces approximately 1.4 nm in height, corresponding well to the 1.3 nm separation of the basal planes of the lattice (Figure 2). Topographs of the monolayer on the R plane (Figure 3) also showed a distribution of step heights in the 1−2 nm range (1.2 nm steps are expected). Excess PA SAM molecules or other loosely bound contaminants were easily swept away by taking a topographic image at low loads (~20−30 nN). The coated amorphous alumina surfaces were much more uniform with reduced topographic variation and no indication of excess PA molecules (Figure 4). That there was no excess material evident in the C-plane and amorphous alumina topographs suggests that PA SAM deposition was more uniform on those surfaces than on the R plane. For all samples, the rms roughness was less than 0.5 nm for an image size of 1 μm^2 (multiple terraces in the image) or smaller and less than 0.1 nm for (100 nm)^2, corresponding to a single terrace.

Results

A. Contact Angle. Contact angle measurements were performed to determine the wettability of the SAMs with polar (water) and nonpolar (hexadecane) liquids. Small contact angles

(29) Varenberg M.; Etsion I.; Halperin G. *Rev. Sci. Instrum.* **2003**, *74*, 3362−3367.

(30) Ogletree, D.; Carpick, R.; Salmeron, M. *Rev. Sci. Instrum.* **1996**, *67*, 3298−3306.

(31) The scripts are available for noncommercial use at http://mandm.engr.wisc.edu/faculty_pages/carpick/toolbox.htm.

(32) Cannara, R. J.; Brukman, M. J.; Carpick, R. W. *Rev. Sci. Instrum.* **2005**, *76*, 053706-1−6.

(33) Watson, G. S.; Dinte, B. P.; Blach-Watson, J. A.; Myhra, S. *Appl. Surf. Sci.* **2004**, *235*, 38−42.

(34) Qian, L. M.; Xiao, X. D.; Wen, S. Z. *Langmuir* **2000**, *16*, 662−670.

(35) Enachescu, M.; van den Oetelaar, R.; Carpick, R.; Ogletree, D.; Flipse, C.; Salmeron, M. *Tribol. Lett.* **1999**, *7*, 73−78.

(36) Carpick, R.; Ogletree, D.; Salmeron, M. *J. Colloid Interface Sci.* **1999**, *211*, 395−400.

(37) The after radii were estimated via the lateral calibration sample. Topographs of the crests of the wedge grating provided an upper bound to the sharpness of the tip. Radii were calculated by fitting parabolas to the topographs ±45 nm on either side of the crest.

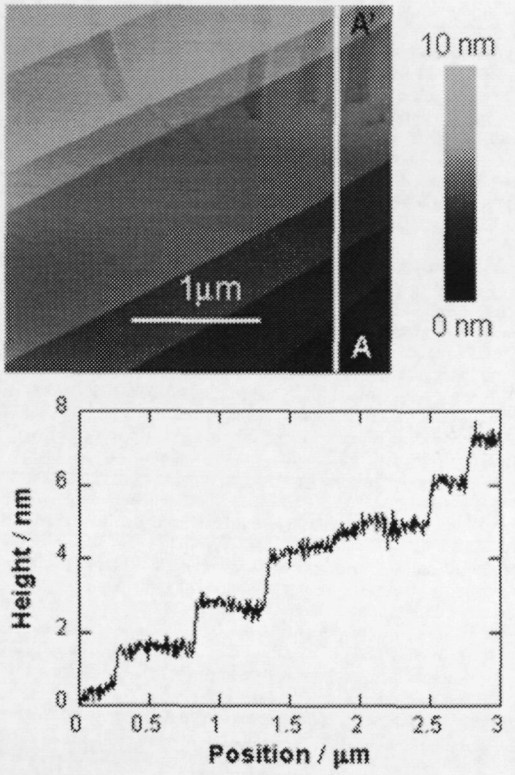

Figure 2. AFM topographic image and cross-sectional profile (from A to A') of $H_{18}PA$ on C-plane sapphire. Adjacent terraces differ in height by 1.2 nm.

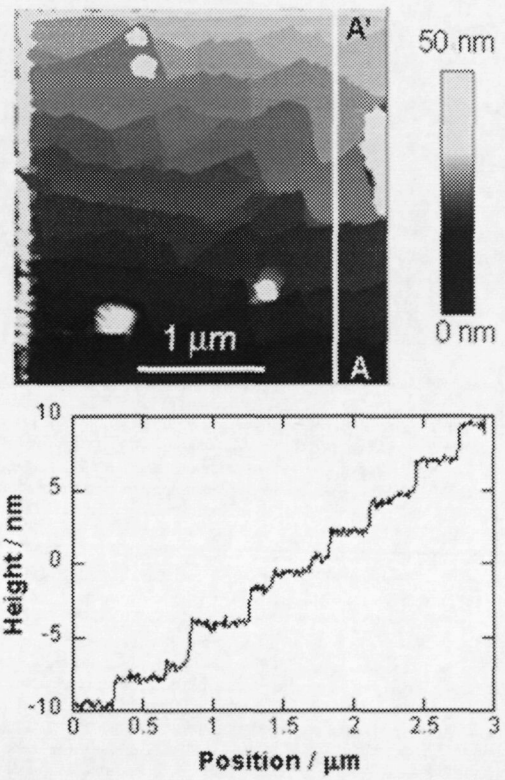

Figure 3. AFM topographic image and cross-sectional profile (from A to A') of $H_{18}PA$ on R-plane sapphire after excess coating (visible as the white bands at the left and top) has been swept aside.

indicate the spreading of the fluid on the SAM whereas large angles indicate that contact between the fluid and SAM is unfavorable. As expected, and without regard to the underlying Al_2O_3 surface, the $F_8H_{11}PA$ SAMs always exhibited greater contact angles with water and hexadecane than did the $H_{18}PA$ SAMs (Tables 1 and 2). Interestingly, there was also less variation for a given contact angle measurement among the three types of alumina for $H_{18}PA$ than for $F_8H_{11}PA$. The variation between substrates within four of the five measurements for each hydrogenated PA was less than the variation in the semifluorinated PA, with the exception being the advancing hexadecane measurement.

B. Tip Contamination. Our initial measurements showed a considerable amount of transient behavior within a set of FL measurements, especially when switching between $H_{18}PA$ and $F_8H_{11}PA$ samples. Tip contamination by the SAM molecules was believed to be the cause, and this was confirmed more directly by scanning an uncoated alumina sample after scanning a SAM-coated sample and observing even more pronounced transient effects. Figure 5 demonstrates the variation in friction as material is added to and then removed from the tip, depending on the sample being scanned. The first FL measurement shown (labeled "0") was obtained with a fresh tip on bare alumina. Subsequently, a series of FL measurements were performed on an $H_{18}PA$ monolayer (not shown; see further below for a comparison of frictional forces between coated and uncoated samples). FL data were immediately taken again on the same alumina surface (chronologically labeled 1–8).

Table 1. Water and Hexadecane Contact Angle Measurements on the $H_{18}PA$ SAM

	water	hexadecane
alumina type	adv/static/rec	adv/rec
C-plane sapphire	113°/106°/80°	41°/37°
R-plane sapphire	112°/106°/82°	39°/36°
amorphous Al_2O_3	114°/109°/89°	38°/31°

Table 2. Water and Hexadecane Contact Angle Measurements on the $F_8H_{11}PA$ SAM

	water	hexadecane
alumina type	adv/static/rec	adv/rec
C-plane sapphire	121°/111°/82°	80°/77°
R-plane sapphire	122°/108°/83°	80°/73°
amorphous Al_2O_3	126°/121°/109°	81°/69°

Friction is seen to be greatly reduced at first but then increases with time. This transient behavior can be explained only by material transfer from the $H_{18}PA$ surface to the tip (between runs 0 and 1) and subsequent removal from the tip by scanning the high-friction bare surface (during scans 1–8). The general implications of this behavior are very important if accurate and reproducible friction measurements with AFM are desired: the tip chemistry may change upon scanning a new sample, and the tip must be brought to steady state before measurements can be considered trustworthy. The extent to which transient frictional behavior occurs may also be a general, qualitative indication of the bonding of SAM molecules to a substrate.

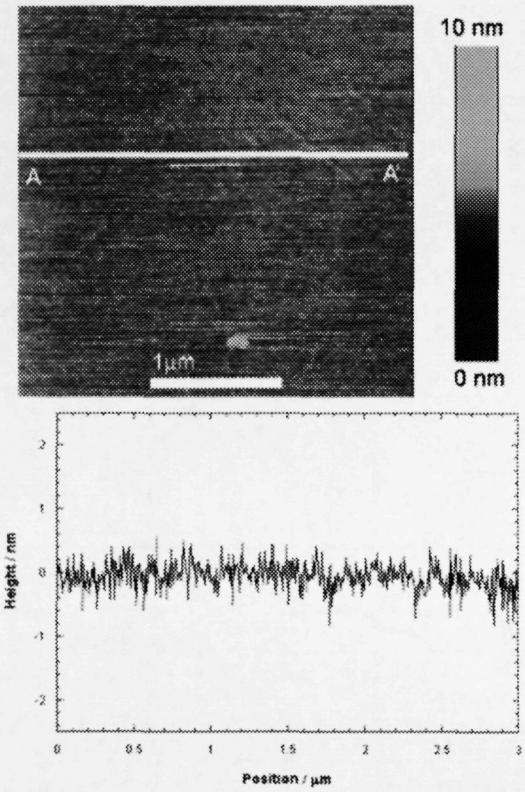

Figure 4. AFM topographic image and cross section (from A to A') of the $F_8H_{11}PA$ SAM on amorphous alumina.

The purpose of the run-in procedure discussed in the Experimental Section is not necessarily to remove material from the tip but to replace material on the tip until it reaches a steady state for that particular surface. The configuration of the material on the tip is simply not known and is extremely difficult to characterize. (There are no established methods for this.) A simple schematic is shown in Figure 6. The primary consequence of this equilibration procedure is that friction and adhesion measurements presented here are not tip-on-SAM but $H_{18}PA$-on-(defective)-$H_{18}PA$ or $F_8H_{11}PA$-on-(defective)-$F_8H_{11}PA$. In other words, we are studying friction, adhesion, and contact evolution processes that are relevant when an uncoated asperity makes contact with a SAM-coated surface. Also, previous friction measurements performed on other SAMs without any confirmation of stable, reproducible behavior may warrant reinterpretation in light of these results on phosphonic acid SAMs.

C. Adhesion. Adhesion measurements were obtained in a number of different sessions of data acquisition. There were large variations in pull-off force measurements, and this occurred on four levels of descending magnitude: (level 1) from experiment to experiment involving different tips, (level 2) from position to position on the same sample during a single experiment using the same tip, (level 3) from one type of measurement to the other (FD or FL), and (level 4) from one type of monolayer ($F_8H_{11}PA$ vs $H_{18}PA$) to the other.

The variation within level 1 is illustrated in the bar graph plot of Figure 7, which shows the variation in pull-off force measured on different days and with different AFM cantilevers/tips,

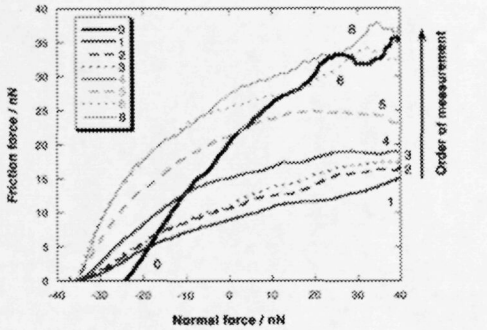

Figure 5. FL measurements on bare amorphous alumina. 0 (solid line) is the response of an unused tip on the bare alumina sample. Then, the tip was scanned on an $H_{18}PA$ sample (acquired data not shown). Subsequent scans (1–8, in order of acquisition) show the response of this used tip on the bare alumina sample again. The frictional forces at each normal force increase with successive measurements, eventually reaching steady state, similar to the original measurement 0, as the SAM molecules are removed from the tip. The larger adhesion force seen in 8 as compared with that in 0 can be explained by an increase in the tip radius. Data set 7 overlapped sets 6 and 8 and is not shown for clarity.

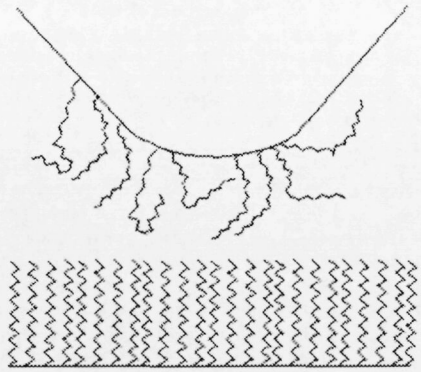

Figure 6. Simple schematic illustrating molecules transferred to the tip. Adsorbed SAM molecules may lie on the surface or may attach to the tip via end groups.

expressed in terms of the work of adhesion, calculated according to DMT contact mechanics.[38] The post-scanning (blunted) tip radii were used for the calculations, so these values represent lower bounds to the work of adhesion. This is aggregate data for all types of alumina substrates because there was little variation in adhesion among the three types of substrates with the same type of SAM on a given day. Approximately equal numbers of measurements were taken for each PA/substrate combination, and the measurements are shown in chronological order.

With tips 0 and 3, $F_8H_{11}PA$ and $H_{18}PA$ are indistinguishable. From the second and third data sets, each taken with tip 2 but separated by 12 h, the $H_{18}PA$ shows distinctly higher adhesion, with the adhesion between $F_8H_{11}PA$ and the tip approximately 55% that of $H_{18}PA$. The laboratory's relative humidity readings during the measurements were as follows: tip 1 = 20%; tip 2, session 1 = 42%; tip 2, session 2 = 45%; tip 3 = not known but believed to be 40–50% on the basis of the consistent known behavior of the laboratory.

(38) Derjaguin, B. V.; Muller, V. M.; Toporov, Y. P. *J. Colloid Interface Sci.* **1975**, *53*, 314–326.

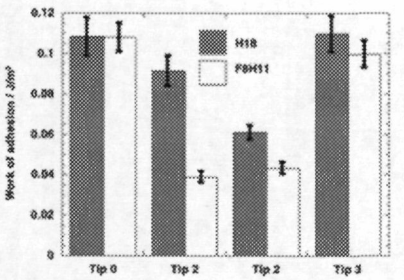

Figure 7. Adhesion measurements of PA SAM films on alumina, measured with a silicon AFM tip. Only one tip was used per pair of data columns. Error bars are 95% confidence intervals. For the four sets of measurements, $N = 250$, 105, 105, and 240, respectively.

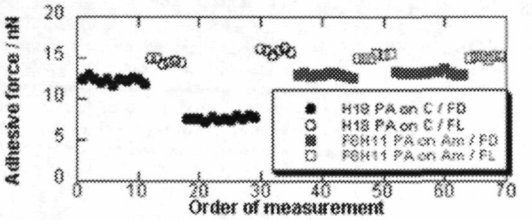

Figure 8. Pull-off force as measured by both force–distance curves and from FL measurements. Adhesion was usually greater during friction measurements and tended to increase with time within a given series of measurements, suggesting that adhesion hysteresis is playing a role.

Levels 2 and 3 of variation (local spatial variation and differences between FD and FL measurements) are evident in the scatter plot of Figure 8 with FD and FL data obtained at two distinct locations from each other, each for $H_{18}PA$ and $F_8H_{11}PA$. FL measurements clearly and consistently yield greater pull-off forces than FD tests. (Data in this Figure are presented in terms of the raw pull-off force rather than the work of adhesion.) Because transfer of material from the SAM to the tip is observed, it is suspected that increased deformation of the tip and sample chain molecules,[39,40] which is facilitated by the increased contact times and compressive nature of the FL measurement, is the cause of this difference between FD and FL measurements.

This difference between FD and FL pull-off forces is consistent with the "adhesion hysteresis" idea of Israelachvili,[41,42] who showed that increased contact time and load for chainlike molecules lead to greater pull-off forces. Indeed, the tip and SAM are in contact for much longer times and sliding distances during FLs (85 s, 26 μm) than during FDs (0.5 s, <200 nm). The difference does not result from the different loading rates used because 0.1 Hz FD measurements showed no difference with FD measurements taken at 2 Hz. Also, in one particular instance, moving from one position to another in the $H_{18}PA$ results in the FD pull-off force being reduced, whereas the FL data remain in relative agreement with those from the previous spot, demonstrating the position-to-position variation in pull-off force. It is possible that the variations could reflect local differences in the SAM packing density, but if so, it is surprising that the FL data were not affected; we therefore suggest that this is unlikely. The variations in pull-off force that we observe require further study that involves the extremely challenging task of identifying the specific chemical nature of the tip as well as its shape and size; they may also reflect local surface or tip contamination.

(39) Nakagawa, T.; Ogawa, K.; Kurumizawa, T. *J. Vacuum Sci. Technol., B* **1994**, *12*, 2215–2218.
(40) Richter, R. P.; Brisson, A. *Langmuir* **2003**, *19*, 1632–1640.
(41) Israelachvili, Adhesion, Friction, and Lubrication of Molecularly Smooth Surfaces. In *Fundamentals of Friction: Macroscopic and Microscopic Processes*; Singer, I. L., Pollock, H. M., Eds.; Kluwer Academic Publishers: Dordrecht, The Netherlands, 1992; Vol. 220, pp 351–385.
(42) Yoshizawa, H.; Chen, Y. L.; Israelachvili, J. *Wear* **1993**, *168*, 161–166

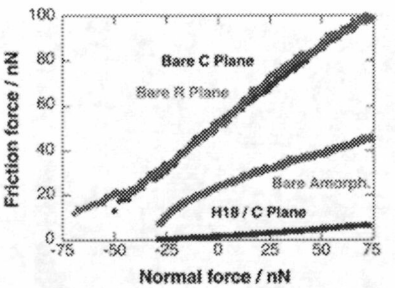

Figure 9. Friction versus load for three bare alumina surfaces and an $H_{18}PA$ film. Each data set represents an average of 10 measurements. Friction for the bare amorphous surface is lower than for the bare crystalline surfaces, likely because of increased ambient contamination because this surface was not furnace annealed. All SAM-coated surfaces, including the one shown here, exhibit friction that is dramatically lower than that for all uncoated surfaces.

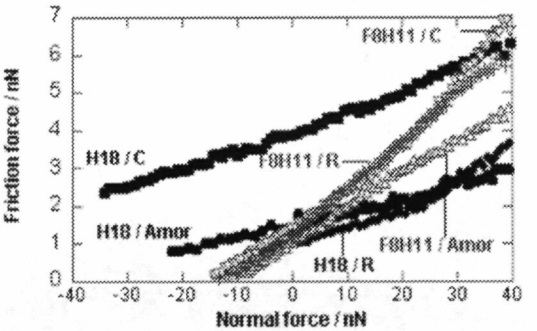

Figure 10. Averages of a series of FL measurements; each is an average of six individual measurements. Only one of every five data points is shown for clarity. Standard errors in frictional force (not shown) extend <4% in each direction.

D. Friction. Most dramatically, the application of a PA monolayer to all three types of bare alumina greatly reduced friction; see Figure 9 for an example of $H_{18}PA$ compared with the three bare substrates. These measurements were taken 1 month after the C- and R-plane sapphire surfaces had been annealed and stored in laboratory air, whereas the amorphous alumina was never annealed. The sapphire substrates are expected to have a more polar and hydrophilic hydroxylated surface than the bare amorphous alumina, but the exact state is not known. Correspondingly, the bare amorphous substrate exhibits significantly less friction and adhesion than the two bare sapphire substrates. Nevertheless, the PA SAM-coated surface exhibits even more dramatically reduced friction. This decrease was observed for all SAMs, for which absolute frictional forces decreased by up to a factor of 20 and the differential friction decreased by factors ranging from 5 to 11, compared with the bare substrates.

Friction also varied systematically with SAM type. Figure 10 shows FL data on all six SAM/substrate combinations, acquired with the same tip. Results from complete sets of FL measurements

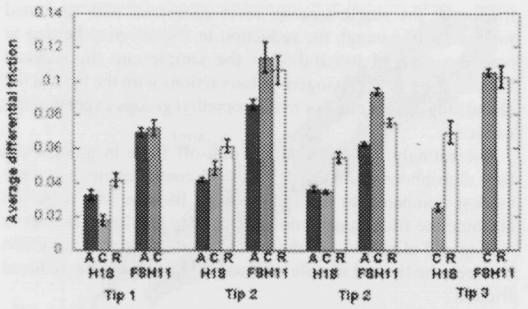

Figure 11. Average differential friction values (α) over a series of measurements involving different tips. (tip 2 was used twice, in the order shown.) A, C, and R correspond to amorphous, C-plane, and R-plane alumina, respectively. Error bars represent 95% confidence intervals. *N* for each tip is 10, 10, 10, and 30.

(all six substrate/SAM combinations) taken with the three tips are shown in Figure 11. Using the average slope of an FL measurement (the single-asperity friction coefficient, α) as the comparative metric, the steeper $F_8H_{11}PA$ curves indicate a larger frictional response for that monolayer as compared to that for $H_{18}PA$. However, larger values of α do not always correspond to larger values of frictional force at a given load because the pull-off force essentially shifts the friction versus load curve to the left. Note that Figure 10 appears to contradict the earlier statement that adhesion does not depend on the substrate, but in fact each FL curve in this example represents only six individual measurements, a small subset of the total number of measurements. As mentioned above, adhesion often varied from location to location and according to the tip condition. Yet surprisingly, these fluctuations in adhesion and, correspondingly, in the frictional force at a given load did not cause α to vary, and we conclude that they do not impede the comparative analysis of the friction measurements. Therefore, we emphasize that our comparisons of frictional response are not necessarily indicative of the magnitude of the frictional force at a given load but rather of the rate of increase of friction with load, which will be discussed further below.

Whereas the absolute slopes α for a given sample changed from tip to tip, they were consistent relative to one another when comparing different samples with the same tip. Specifically, independent of the tip and the adhesion forces, α for $H_{18}PA$ was 30−60% that of α for $F_8H_{11}PA$ on the same substrate. To account for the tip shape and laboratory environment and demonstrate trends among the SAM−substrate pairs, the values of α may be normalized by the value of α of $H_{18}PA$ on the C-plane ($\alpha_{C,H}$) for that session, as shown in Table 3, which reports aggregate data for all tips.

To a lesser extent, α also depended on the type of alumina underneath the SAM. Both $H_{18}PA$ and $F_8H_{11}PA$ monolayers on amorphous alumina (labeled "A" in Figure 11) had a lower α than those on the R sapphire, although for the fluorinated case we were able to make a comparison only between these two substrates for tip 2. The trend was clear and consistent with both sets of measurements using tip 2. $F_8H_{11}PA$ films on amorphous alumina also exhibited α values as low as or lower than those on C-plane sapphire. Comparisons of α for $H_{18}PA$ on C-plane sapphire and amorphous alumina were inconsistent from tip to tip. Furthermore, for $H_{18}PA$ films, the C-plane sapphire exhibited consistently lower α values than the R plane. In contrast, the C and R planes were generally indistinguishable from each other for $F_8H_{11}PA$ SAMs. In summary, we find that the effect of the substrate can be expressed as follows:

Table 3. Values of the Single-Asperity Friction Coefficient Relative to $H_{18}PA$ on the C Plane of Sapphire

SAM/substrate	normalized α (95% confidence)
$H_{18}PA$/C plane	1.0 ± 0.4
$H_{18}PA$/amorphous	1.2 ± 0.1
$H_{18}PA$/R plane	2.2 ± 0.4
$F_8H_{11}PA$/amorphous	2.6 ± 0.2
$F_8H_{11}PA$/R plane	3.2 ± 0.9
$F_8H_{11}PA$/C plane	3.6 ± 0.6

(1) For the $H_{18}PA$ films, we consistently find that $\alpha_A < \alpha_R$ and $\alpha_C < \alpha_R$, but we do not find a consistent, significant difference between α_A and α_C. This indicates that for hydrogenated films the R plane has a modestly unfavorable effect on friction.

(2) For the $F_8H_{11}PA$ films, we consistently find that $\alpha_A < \alpha_C$, although in one of the three cases the difference is not statistically significant. For both sets of measurements with tip 2, we find that $\alpha_A < \alpha_R$. We also find that α_C is either equivalent to or greater than α_R. This indicates that for semifluorinated films the amorphous substrate has a modestly favorable effect on friction.

Discussion

A. Contact Angle and Film Structure. Contact angle measurements, through comparison with previous literature studies, can provide insights into the structure of SAMs. First, we discuss the results for semifluorinated films. Dynamic contact angle data have been reported for $F_8H_{11}PA$ SAMs on the native oxide of vapor-deposited aluminum[10,43] and for $CF_3(CF_2)_7(CH_2)_{11}PO_3H_2$ ($F_8H_{11}PA$ in our shorthand) on vapor-deposited alumina.[44] In accord with those studies and previous studies of similar semifluorinated alkanethiol SAMs on gold,[17,45−47] the advancing and static contact angle data for water and hexadecane reveal that $F_8H_{11}PA$ exposes CF_3 groups to the air/film interface.

The water receding contact angles reported for our semifluorinated films are lower than those reported for $F_8H_{11}PA$ on aluminum's native oxide and for $F_{10}H_{11}SH$ on Au (by ~10° for amorphous alumina and ~35° for crystalline), meaning that there is more contact angle hysteresis. Larger hysteresis has been linked to more penetration of the probe liquid into the SAM[48] (e.g., via pinholes in monolayer coverage) and has been reviewed in detail by Chaudhury[49] and references therein. Furthermore, greater hysteresis has been correlated with an increased amount of translational disorder[50] and decreased alkyl chain coverage[51] in alkanethiol SAMs on Au. The lower water contact angle values suggest that our $F_8H_{11}PA$ SAMs have somewhat lower coverage than those prepared on aluminum's native oxide[10] or of $F_{10}H_{11}SH$ on gold.[46] In comparing the data in this study for receding contact angles of water on $F_8H_{11}PA$ on the three substrates, films on R- and C-plane sapphire exhibit smaller advancing contact

(43) We note that those vapor-deposited metal surfaces consist of "irregularly shaped grains...from 0.3 to 1.0 mm" and are much rougher (as measured by AFM) than the alumina or sapphire used here.

(44) Kelley, T. W.; Boardman, L. D.; Dunbar, T. D.; Muyres, D. V.; Pellerite, M. J.; Smith, T. Y. P. *J. Phys. Chem. B* **2003**, *107*, 5877−5881.

(45) Tsao, M.; Hoffmann, C.; Rabolt, J.; Johnson, H.; Castner, D.; Erdelen, C.; Ringsdorf, H. *Langmuir* **1997**, *13*, 4317−4322.

(46) Fukushima, H.; Seki, S.; Nishikawa, T.; Takiguchi, H.; Tamada, K.; Abe, K.; Colorado, R.; Graupe, M.; Shmakova, O. E.; Lee, T. R. *J. Phys. Chem. B* **2000**, *104*, 7417−7423.

(47) Frey, S.; Heister, K.; Zharnikov, M.; Grunze, M.; Tamada, K.; Colorado, R.; Graupe, M.; Shmakova, O. E.; Lee, T. R. *Isr. J. Chem.* **2000**, *40*, 81−97.

(48) Timmons, C. O.; Zisman, W. A. *J. Colloid Interface Sci.* **1966**, *22*, 165−171.

(49) Chaudhury, M. K. *Mater. Sci. Eng., R* **1996**, *16*, 97−159.

(50) Lestelius, M.; Engquist, I.; Tengvall, P.; Chaudhury, M. K.; Liedberg, B. *Colloids Surf., B* **1999**, *15*, 57−70.

(51) Park, J. S.; Vo, A. N.; Barriet, D.; Shon, Y. S.; Lee, T. R. *Langmuir* **2005**, *21*, 2902−2911.

angles and more hysteresis than those on amorphous alumina, meaning that there is higher coverage on the latter, suggesting a higher packing density and perhaps more translational ordering of the $F_8H_{11}PA$ SAM on the amorphous alumina.

The pure hydrocarbon SAMs reported here yield advancing and static contact angles consistent with the expression of the $-CH_3$ group at the air/film interface.[10,44,52,53] The advancing and static angles reported here for water are close to those for $H_{16}PA$ on aluminum's native oxide[10] and $H_{16}PA$ applied to amorphous alumina through a spin-coat and heat procedure.[44] Once again, the receding water contact angle values in our study are lower than those in previous studies (by ~10°), suggesting a somewhat lower coverage of $H_{18}PA$ in this study. In general, the reduced contact angles in this study as compared to those in previous work on films formed on the native oxide of aluminum may result from lower SAM coverage on the amorphous and crystalline alumina surfaces driven by the lower reactivity of these surfaces relative to the native oxide of aluminum.

We note here a subtle difference in contact angles between $H_{18}PA$ on these substrates and what is typically observed for SAMs of long-chain alkanethiols on gold. Whereas the advancing water contact angles reported here are essentially identical to what has been reported for thiols on gold (110−115°), advancing hexadecane contact angles are significantly lower (50−52° for thiols,[50,51] 38−41° for our work). Data from the literature have shown that water has an advancing angle of ~113° for a methyl surface, whereas on a methylene surface it is reduced to only ~103°.[54,55] Hexadecane, however, has an advancing contact angle of ~51° on a methyl surface, whereas it wets a methylene surface. Consequently, hexadecane is a more sensitive probe of the methylene content of a surface than is water. Whereas our advancing angles indicate a mostly methyl-terminated surface, which is nearly the same as that of long-chain alkanethiols on gold, the hexadecane advancing contact angles indicate that there is some degree of additional methylene content at the surface in our $H_{18}PA$ on sapphire and amorphous alumina than there is for alkane thiols on gold, consistent with the notion that the coverage is somewhat lower. Lower contact angles may also indicate a higher tilt angle from the surface normal. Advancing hexadecane contact angles with our $F_8H_{11}PA$ (80−81°) very nearly reproduce measurements of partially fluorinated thiols from the literature (e.g., 79° for F_8H_2SH[13] and 83° for F_8H_8SH[56]).

The PA SAMs are favorable to thiols in terms of longevity and stability. Whereas thiols on gold and silver oxidize and degrade with time in a matter of weeks,[57] the PA SAMs examined here were stable for the six months that elapsed between deposition and final AFM imaging; during that time, they were stored in an ambient laboratory atmosphere. The substrates were eventually reused for infrared spectroscopy measurements on the SAMs, so the maximum lifetime of these alumina/PA SAM pairs has not yet been determined.

B. Nanotribology of Bare versus Coated Samples. As expected, coating alumina surfaces with PA SAMs reduces friction (both in absolute force and differential friction α) at the single-asperity level, and the reduction is dramatic. This clearly demonstrates the effectiveness of PA SAMs in reliably reducing friction at the single-asperity level compared with uncoated substrates. In general, the reduction in friction may be due to both the reduced wettability of the sample and the reduced attractive normal and tangential interactions with the tip that the chemically inert methyl or trifluoromethyl groups express at the surface.

Interestingly, the reduction in pull-off force in going from bare amorphous alumina to PA SAM-coated alumina is very modest compared to the reduction in friction. We therefore attribute the friction reduction exclusively to a lower barrier to sliding and eliminate any decrease in contact area or attraction between the tip and sample as a possible cause for the reduced friction.

The low friction behavior persisted over the 6 months that the samples were studied, indicating far better tribological stability than for thiols on gold or silver.[6,57] The range of values of the work of adhesion, 0.040−0.12 J/m^2, is comparable to other measurements for silicon tips on SAMs[58] and includes the value measured for self-mated CH_3-on-CH_3 interfaces.[59] 0.060 J/m^2.

The reduced friction of bare amorphous alumina as compared to that of bare annealed sapphire seen in Figure 9 suggests that there is an increased amount of passivating adventitious carbon adsorbed from ambient exposure on the former. Nevertheless, the addition of the PA SAM still reduces differential friction by a factor of at least 5 beyond the lubrication provided by such contamination.

C. Effect of Fluorination on Nanotribology. In comparing different PA SAM films with each other, the most noticeable contrast is the pronounced increase in differential friction α in going from $H_{18}PA$ to $F_8H_{11}PA$ monolayers. Typically, there was also greater absolute friction at positive loads for the F_8H_{11} PA, with variations in adhesion resulting in outlying high absolute friction measurements for $H_{18}PA$, as seen, for example, in Figure 10. This is in agreement with previous results from other experimental and molecular dynamics studies of alkanethiols on gold,[14,60−63] although in these studies only the terminal group was fluorinated whereas the rest of the chain was strictly alkane. Here, the slope of the friction vs load data differed by a factor of ~1.5−3.6, depending on the substrate, whereas previous work on alkanethiols reported factors of 3 to 4. We note that our work is the first where friction and load forces are experimentally calibrated *in situ*.

The difference in friction between pure alkanes and $-CF_3$-terminated alkanes has been attributed previously to the greater size of the terminal CF_3 groups compared to that of CH_3 groups. Because only the terminal group was fluorinated in the previous studies, the packing densities of the two types of chains were identical, and equal numbers of large CF_3 groups were packed into the same area as CH_3 groups, imposing a significant barrier to CF_3 group motion (i.e., deformation and rotation). In the MD simulations of self-mated SAM interfaces by Park et al.,[60] this leads to higher ordering of the CF_3 groups in the film, and this is correlated with higher frictional forces. However, in our case, the top 8 out of 19 carbons are fluorinated, precluding such a direct comparison of the data. A different possible origin of this contrast is discussed further below.

(52) Bain, C. D.; Troughton, E. B.; Tao, Y. T.; Evall, J.; Whitesides, G. M.; Nuzzo, R. G. *J. Am. Chem. Soc.* **1989**, *111*, 321−335.
(53) Liakos, I. L.; Newman, R. C.; McAlpine, E.; Alexander, M. R. *Surf. Interface Anal.* **2004**, *36*, 347−354.
(54) Atre, S. V.; Liedberg, B.; Allara, D. L. *Langmuir* **1995**, *11*, 3882−3893.
(55) Allara, D. L.; Atre, S. V.; Elliger, C. A.; Snyder, R. G. *J. Am. Chem. Soc.* **1991**, *113*, 1852−1854.
(56) Weinstein, R. D.; Moriarty, J.; Cushnie, E.; Colorado, R., Jr.; Lee, T. R.; Patel, M.; Alesi, W. R.; Jennings, G. K. *J. Phys. Chem. B* **2003**, *107*, 11626.
(57) Leggett, G. J. *Anal. Chim. Acta* **2003**, *479*, 17−38.
(58) Burns, A. R.; Houston, J. E.; Carpick, R. W.; Michalske, T. A. *Phys. Rev. Lett.* **1999**, *82*, 1181.
(59) Thomas, R. C.; Houston, J. E.; Crooks, R. M.; Kim, T.; Michalske, T. A. *J. Am. Chem. Soc.* **1995**, *117*, 3830−3834.
(60) Park, B.; Lorenz, C. D.; Chandross, M.; Stevens, M. J.; Grest, G. S.; Borodin, O. A. *Langmuir* **2004**, *20*, 10007−10014.
(61) Kim, H. I.; Graupe, M.; Oloba, O.; Koini, T.; Imaduddin, S.; Lee, T. R.; Perry, S. S. *Langmuir* **1999**, *15*, 3179−3185.
(62) Graupe, M.; Koini, T.; Kim, H. I.; Garg, N.; Miura, Y. F.; Takenaga, M.; Perry, S. S.; Lee, T. R. *Colloids Surf., A* **1999**, *154*, 239−244.
(63) Kim, H. I.; Koini, T.; Lee, T. R.; Perry, S. S. *Tribol. Lett.* **1998**, *4*, 137−40.

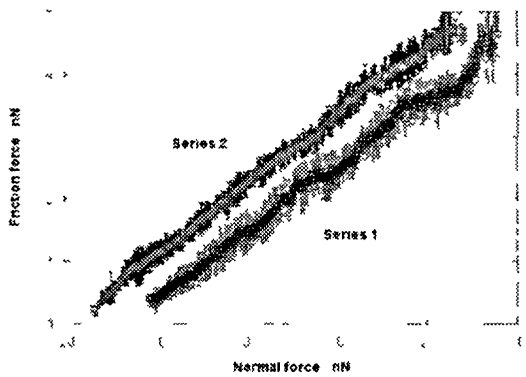

Figure 12. [illegible] friction data at two nearby locations. 95% confidence intervals, N = 5.

D. Linearity of Friction versus Load. Several previous studies have reported that single-asperity frictional forces are often proportional to the true area of contact,[55,64–78] which for a single parabolic asperity between homogeneous, isotropic, linear, elastic materials as well as in many other cases varies in a nonlinear fashion with the load in a characteristic, well-defined manner.[79] This type of load dependence was rarely seen over the course of these experiments, as the individual FL plots typically were almost always highly linear, as seen in Figures 10 and 12.

Furthermore, consistent with the adhesion measurements described above, the FL measurements exhibit a local variation in the pull-off force (Figure 12). After FL measurements were performed at one position, the cantilever was moved to another spot, and another series was performed. Whereas the pull-off force increased by 50% from one position to another, the average differential friction α varied by less than 5%, validating the use of α as the figure of merit for comparing friction measurements. We believe that the consistency in this figure, despite the variations in absolute frictional force and adhesion force, is a rather remarkable demonstration of independent contributions to the total frictional behavior of an interface.

The linearity in the friction vs load data and the lack of dependence of α on the pull-off force can be explained by one of two hypotheses: (1) the shear strength is pressure dependent or (2) friction is dominated by molecular plowing. The first hypothesis is motivated by the observation that single-asperity contacts demonstrate frictional forces F proportional to the interfacial shear strength τ and the true contact area A (i.e., $F = \tau A$[80]). Expressing the shear strength dependence on the mean normal contact pressure to first order[12] yields $\tau = \tau_0 + \alpha L/A$ and therefore $F = \tau_0 A + \alpha L$. When the second term dominates, FL plots are nearly linear. Thus, α represents the shear strength's dependence on mean contact pressure and is the figure of merit for friction. Because the AFM measures the response of the normal and shear contact stresses averaged over the entire tip–sample junction and because the contact area drops out of the force equations above, this analysis of α is independent of the length scale of the contact (i.e., the radius of the tip). This may not be the case in general, especially for large ranges of tip radius and normal load.

This linear dependence has been suggested to be a manifestation of the Eyring activation model,[3,81,82] whereby the effect of increased normal contact pressure is to modify the conformation of the materials at the interface and to correspondingly create a larger energy barrier to sliding, thus increasing the frictional force per area (interfacial shear strength). This is expected to be a significant effect for softer materials such as polymers and SAMs, where pressure readily induces changes in the molecular conformation at the interface. However, for solids, where no such conformational change with applied pressure occurs, the interfacial shear strength remains constant as the pressure is increased, as long as the materials are only elastically deformed. Hence, the observation of linear FL behavior may be indicative of the fact that conformational changes, such as gauche defects, are being induced to an increasing degree as the load is increased, and this increases the shear strength. This is precisely what is observed in a recent molecular dynamics simulation of friction sliding for alkane-based SAM-coated surfaces.[84]

The second hypothesis is of a significantly different physical origin. Unlike two stiff solids sliding against each other, such as bare SiO_2 and Al_2O_3, the SAM layers are compliant and anisotropic on the atomic scale. Weak van der Waals forces between adjacent chains mean that displacements normal to the surface are localized (i.e., decoupled from their neighbors). Thus, one would not expect the SAM to be deformed as significantly outside of the contact region as an isotropic elastic solid would. However, the monolayer is densely packed in-plane, so lateral (shear) deformation will couple to molecules beyond the contact zone. If the compressive normal (vertical) deformation is localized only to the molecules immediately underneath the tip, then the act of sliding involves molecular-scale plowing. Because the tip lies below the top surface of neighboring PA molecules (Figure 13), the tip must either compress or laterally deform adjacent molecules in the forward direction to slide. As the load increases, the tip penetrates the monolayer by an increasing amount and encounters a greater physical barrier to motion because it must deform more material at high loads than low loads. From geometry, when a paraboloidal tip penetrates a flat surface, the projected contact area A_P of the tip along an in-plane direction (that is, the area of a 2-D parabola of curvature R), up to height

(64) Carpick, R. W.; Ogletree, D. F.; Salmeron, M. *J. Colloid Interface Sci.* **1999**, *211*, 395–400.
(65) Singer, I. L.; Pollock, H. M. *Fundamentals of Friction: Macroscopic and Microscopic Processes*; Kluwer: Dordrecht, The Netherlands, 1992.
(66) Singer, I. L. Solid lubrication processes. In *Fundamentals of Friction: Macroscopic and Microscopic Processes*; Singer, I. L., Pollock, H. M., Eds.; Kluwer: Dordrecht, The Netherlands, 1992; Vol. 220, p 237.
(67) Carpick, R. W.; Agraït, N.; Ogletree, D. F.; Salmeron, M. *Langmuir* **1996**, *12*, 3334–3340.
(68) Carpick, R. W.; Agraït, N.; Ogletree, D. F.; Salmeron, M. *J. Vacuum Sci. Technol. B* **1996**, *14*, 1289–1295.
(69) [illegible] *J. Vacuum Sci. Technol. B* **1996**, *14*, 1289–1231.
(70) Carpick, R. W.; Salmeron, M. *Chem. Rev.* **1997**, *97*, 1163–1194.
(71) Lantz, M. A.; O'Shea, S. J.; Welland, M. E.; Johnson, K. L. *Phys. Rev. B: Condens. Matter* **1997**, *55*, 10776–10785.
(72) Lantz, M. A.; O'Shea, S. J.; Welland, M. E. *Phys. Rev. B: Condens. Matter* **1997**, *56*, 15345–15352.
(73) Johnson, K. L. *Proc. R. Soc. London, Ser. A* **1997**, *453*, 163.
(74) Enachescu, M.; van den Oetelaar, R. J. A.; Carpick, R. W.; Ogletree, D. F.; Flipse, C. F. J.; Salmeron, M. *Phys. Rev. Lett.* **1998**, *81*, 1877–1880.
(75) Carpick, R. W.; Enachescu, M.; Ogletree, D. F.; Salmeron, M. Making, Breaking and Sliding of Nanometer-Scale Contacts. In *Fracture and Ductile vs. Brittle Behavior—Theory, Modeling and Experiment*; Beltz, G. E., Kim, K.-S., Selinger, R. L. B., Eds.; Materials Research Society: Warrendale, PA, 1999; pp 93–103.
(76) [illegible] Z.; Wang, C.; Bai, C. *Langmuir* **2001**, *17*, [illegible].
(77) Piétrement, O.; Troyon, M. *Langmuir* **2001**, *17*, 6540–6546.
(78) Piétrement, O.; Troyon, M. *Surf. Interface Anal.* **2001**, *31*, 1060–1067.
(79) Johnson, K. L. *Contact Mechanics*; Cambridge University Press: Cambridge, U.K., 1985; p 9[illegible].
(80) Carpick, R. W.; Agraït, N.; Ogletree, D. F.; Salmeron, M. *J. Vacuum Sci. Technol. B* **1996**, *14*, 1289–1295.
(81) Eyring, H. *J. Chem. Phys.* **1935**, *3*, 107.
(82) Eyring, H. *J. Chem. Phys.* **1936**, *4*, 283.
(83) McDermott, M. T.; Green, J.-B. D.; Porter, M. D. *Langmuir* **1997**, *13*, 2504–2510.
(84) Tutein, A. B.; Stuart, S. J.; Harrison, J. A. *Langmuir* **2000**, *16*, 291–296.

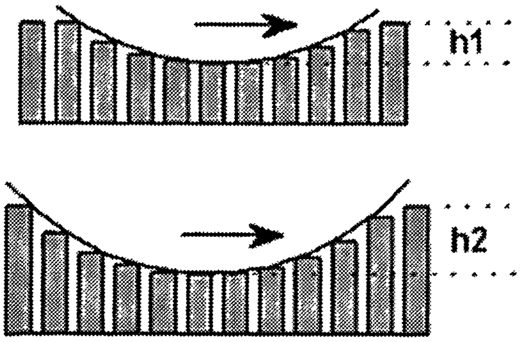

Figure 13. van der Waals interaction between the chains is weak, allowing individual molecules to deform independently along their vertical axes. The AFM tip therefore compresses molecules locally, penetrating the original surface plane of the film by a depth *h*. Some degree of plowing is required for lateral motion, requiring compressing or laterally deforming molecules in the forward neighboring direction over the penetration depth. The work required to slide laterally is proportional to the work required to compress or laterally deform the forward neighboring molecules. Tip penetration is greater at high loads (h2) than low loads (h1), and the shear strength of the interface increases with load.

h) is proportional to $\sqrt{Rh^3}$. For a contact that is Hertzian or weakly adhesive (such as a DMT contact), the normal load *L* associated with the penetration depth *h* is $L = \frac{4}{3}E^*\sqrt{Rh^3}$, where E^* is the reduced modulus of the contact.[85] Therefore, the projected area A_P is proportional to L/E^* and independent of *R*. Furthermore, an increase in adhesion simply adds to the total load, and the linear dependence between the total load and projected contact area remains the same. If we postulate that plowing dominates over interfacial sliding (i.e., that friction is proportional not the to in-plane tip–surface contact area but to the contact area projected onto the vertical plane), then $F = \tau_P A_P$ and friction will be linearly proportional to the load. The physical basis for this postulate is that frictional energy dissipation is not due to the sliding of molecules past one another at the contact interface but to the mechanical deformation of the forward neighboring molecules. This is essentially a molecular-scale manifestation of viscoelasticity; a portion of the energy expended to deform the molecules mechanically (in this case, to allow the tip to move forward) is not recovered but is instead dissipated.

It is not possible, without further complementary experiments and perhaps detailed simulations, to determine which, if either, of the two hypotheses described above applies here. However, it is clear that the simple model of interfacial friction for single asperities, where friction is proportional to the contact area and a constant interfacial shear strength, does not apply here and that the slope of the FL curve is a key indicator of the mechanism of frictional energy dissipation.

E. Effect of the Substrate on the Nanotribological Response. Epitaxial effects are believed to be the cause of the more subtle but nonetheless reproducible dependence of friction upon the substrate for both PA SAMs. Using the van der Waals radii values of Tamada,[17] lower bounds of the surface areas required per CH_2 and CF_2 chain are 0.156 and 0.278 nm², respectively. This means that the $H_{18}PA$ chain is smaller in cross section than the repeating surface area of the two crystalline alumina substrates (0.196 and 0.244 nm² for C and R, respectively), so the availability of packing sites for $H_{18}PA$ chains should be the limiting factor for packing density and the C-plane should support a denser coating. Additionally, the O–O distances in the sapphire basal

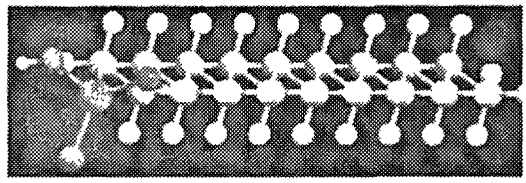

Figure 14. End-on view of an entire isolated PA molecule, showing the tetragonal arrangement of the O and P atoms in the headgroup. The headgroup is on the left, in the foreground.

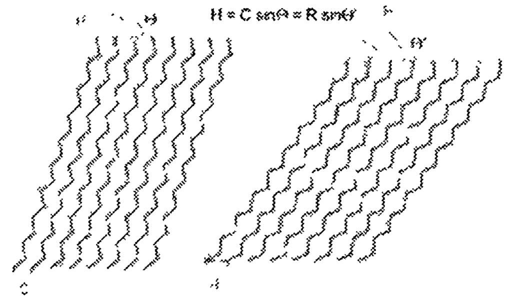

Figure 15. Packing of $H_{18}PA$ on C and R planes of sapphire, assuming (1 × 1) epitaxy. The chains maintain the equilibrium van der Waals spacing (denoted H) for both surface meshes by changing the tilt angle according to the surface bonding site density.

plane (0.27 nm) are very close to the spacing of the single-bonded terminal O's of the phosphonic acid group (0.28 nm) as calculated by Chem3D (CambridgeSoft Corp., Cambridge, MA) (Figure 14, which shows the entire molecule, with the headgroup in the foreground). Thus, a (1 × 1) epitaxial relationship between the $H_{18}PA$ headgroups and the C- and R-plane unit cells is likely and would lead to a nearly ideally packed monolayer on the former and a less dense monolayer on the latter (Figure 15). The lower density would lead to a larger tilt angle of the molecules. The reduced friction that we observe for the C plane compared with that for the R plane of the $H_{18}PAs$ is therefore consistent with previous reports of increased packing density of alkanethiol SAMs correlating with a reduction in friction.[32,86] Furthermore, a comparison of the friction data between the R-plane and amorphous alumina suggests that, on average, surface bonding sites are closer together in the aperiodic distribution of the latter than in the R-plane of sapphire and are comparable to that of the C-plane.

However, a single $F_8H_{11}PA$ chain requires more area (0.278 nm²) than either repeating surface mesh for the C and R planes, preventing an ordered (1 × 1) epitaxial arrangement of the PA molecules; the SAM molecules are simply too large for efficient (1 × 1) packing on the crystalline surfaces. The next largest repeating surface units, (√2 × √2) for R and (√3 × √3) for C, are large enough for a CF_3 chain but at a less-than-ideal packing density. Also, each $F_8H_{11}PA$ molecule has two diameters competing to determine the packing order, with the longer hydrogenated section seeking a much closer packing with its neighbors via van der Waals interactions than the bulkier fluorinated section can accommodate. Figures 16 and 17 demonstrate how the $F_8H_{11}PA$ monolayers may organize on the C and R planes when either the CH_2 or CF_2 segments dominate the packing, respectively.

(85) Lee, S.; Shon, Y. S.; Colorado, R.; Guenard, R. L.; Lee, T. R.; Perry, S. S. *Langmuir* 2000, *16*, 2220–2224.
(86) Liu, X.; Chanda, D. H.; Salmeron, M. *J. Phys. Chem. B* 1997, *101*, 3800–3805.

3998 *Langmuir*, Vol. 22, No. 9, 2006 Brukman et al.

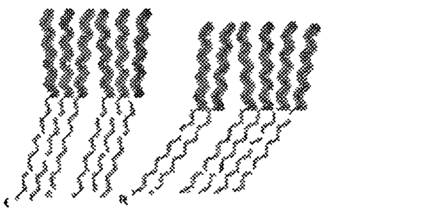

Figure 16. Packing of F_8H_{11} SAMs on the C and R planes of sapphire for the case where the CH_2 segments dominate, maintaining equilibrium spacing. Fluorinated portions of the chain are distorted.

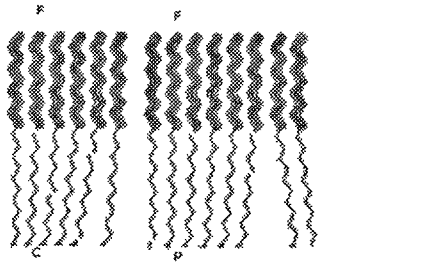

Figure 17. Packing of F_8H_{11} SAMs on the C and R planes of sapphire for the case where the CF_2 segments dominate, maintaining equilibrium spacing. Hydrogenated portions of the chain are distorted. F, C, and R represent the repeat distances for CF_2 packing and unit meshes of C, R plane sapphire.

Frey et al.[87] have studied this topic using similar molecules ($F_{10}H_2$, $F_{10}H_{11}$, and $F_{10}H_{17}$ alkanethiols), using Au and Ag substrates to dictate surface periodicity. There, the surface mesh was also larger than the CH_2 segments and smaller than the CF_2 segments. The absolute tilt angle of the CF_2 chains (relative to the surface normal rather than the CH_2 segments) was not affected by the substrate but did increase with the number of CH_2 segments. Longer molecules had more CH_2–CH_2 van der Waals interactions and behaved more like unfluorinated thiols. On the basis of the results of that paper, we believe that the $F_8H_{11}PA$ SAM's packing structure is closer to that at the end of the spectrum where CH_2 segments dominate (Figure 16). Although the question of how the CH_2 and CF_2 segments accommodate each other depending on substrate crystallinity is an interesting one, this discussion should not detract from our conclusion that the small size of the surface meshes relative to the size of the CF_2 groups imposes a suboptimal packing arrangement. The amorphous alumina, however, does not necessarily impose poor registry between the bonding sites and the PA molecules.

Comparing the friction data for $F_8H_{11}PA$ on amorphous alumina with $F_8H_{11}PA$ on crystalline alumina, we therefore conclude that the packing density is somewhat greater on the former, resulting in the observed reduction in friction. The differences in contact angle measurements between amorphous and crystalline substrates for the fluorinated films indicate greater packing density on the amorphous surfaces, bolstering this conclusion.

There is another explanation for $F_8H_{11}PA$ having lower friction on the amorphous substrate. Molecular dynamics simulations[87,88] have linked higher interfacial ordering and commensurability with higher friction. This implies that these monolayers retain the order of the substrates, despite the incommensurability of the SAM and crystal. If this is the case, then it would come at the cost of reduced packing density.

Conclusions

Static and advancing contact angle measurements performed with water and hexadecane are consistent with previous reports of PA SAMs on aluminum oxide substrates, showing that both $H_{18}PA$ and $F_8H_{11}PA$ SAMs render alumina surfaces highly hydrophobic. However, receding measurements here are generally lower with these samples, suggesting that somewhat lower coverage is attained here than previously reported.[8,1] The contact angle data also suggests that $F_8H_{11}PA$ has a somewhat higher packing density and/or ordering on the amorphous substrate compared to that of the crystalline substrates. The topographic and tribological properties of the SAMs were stable in a laboratory environment for at least 6 months, indicating their high degree of ambient environmental stability, which is far greater than that for alkanethiols.

AFM topographs show that PA SAMs on annealed sapphire and vapor-deposited alumina are smooth and uniform. Loosely bound contaminants or nonbonded PA molecules that were not removed by an ethanol rinse are observed for films on R-plane sapphire, and these are readily swept aside during contact mode AFM scanning to reveal the atomic steps of the underlying single crystal sapphire substrate. Contamination of the tip by the monolayer is observed for all films, leading to transient effects in nanotribology measurements unless the tip and sample are brought to a steady state via a run-in process that we believe coats the tip with a defective layer of PA molecules. Our interfaces can therefore be considered to be nearly self-mated, but experiments with tips deliberately coated with SAMs in a deposition process will be required to verify this hypothesis.

Adhesion between PA SAMs and processed silicon AFM tips is influenced by partial fluorination, and friction is influenced both by fluorination and the surface arrangement of the alumina substrate. Specifically, adhesion between processed tips and $F_8H_{11}PA$ ranged from 50 to 100% of that for $H_{18}PA$ and was never larger. The force–distance technique of adhesion measurement consistently yielded reduced values of the pull-off force compared with those from the friction versus load technique. The compression of chains on the tip and sample resulting from more vigorous contacts between the two in the latter method may be the cause of this effect, along the lines of previous reports of adhesion hysteresis.

Both types of SAMs demonstrated a large reduction in friction compared with the friction of all bare alumina substrates. Furthermore, single asperity friction coefficients for fully hydrogenated SAMs were consistently less by 40–70% than the corresponding values for semifluorinated SAMs. Also, the linear nature of the friction versus load measurements indicates that either the interfacial shear strength is pressure-dependent or that friction is governed by the plowing of the tip through greater depths of the SAM with increasing load.

Whereas applying SAMs greatly reduced the friction for all substrates, some trends within a given SAM type indicate a second-order effect arising from the choice of alumina substrate. Friction is generally lower for amorphous substrates than crystalline ones, whereas differentiation between the C and R planes suggests that steric and epitaxial effects play a small but observable role in the packing and subsequent frictional response of the SAMs.

Acknowledgment. This work was supported by the National Science Foundation (CAREER Award No. CMS-0134571).

LA052847K

(87) [illegible] M.; Webb, E. B.; Stevens, M. J.; Grest, G. S.; Garofalini, S. H. *Phys. Rev. Lett.* 2004, 93, [illegible]

(88) [illegible] *Chem. Rev.* 2008, [illegible]

4.6.6 Lateral Force Microscopy Study of Langmuir-Blodgett Films of a Macrocyclic Compound

G. Oncins[a], J. Torrent-Burgués[b], F. Sanz[a]

[a]Department of Physical Chemistry, Universitat de Barcelona and Center of Nanobioengineering of Catalonia (CREBEC), Martí i Franquès 1, 08028 Barcelona, Spain

[b]Department of Chemical Engineering, Universitat Politècnica de Catalunya, Colom 1, 08222, Terrassa (Barcelona), Spain

Tribology Letters 21(3) (2006), 175-184.

4.6.6.1 Summary

As we have seen, organic monolayers can be used in MEMS and NEMS as extremely sensitive sensors. In the case of this work, we studied Langmuir-Blodgett monolayers of one macrocyclic compound that proved to be a copper sensor. Nevertheless, our main goal in this work was to see if LFM was able to discern between monolayers extracted at different surface pressures. As you may know, there is a certain controversy about the surface pressure of Langmuir films once they have been transferred to a substrate. Do they maintain the molecular area they have on liquid subphase or perhaps they relax to reach an equilibrium pressure? The obtained conclusions can be summarized as follows:

- *AFM topographic study of the tiomacrocycle monolayers demonstrate that the structure of the film once it has been transferred to mica depends on the extraction pressure. The presence of islands is observed and a model to explain its formation is proposed.*

- *F_f vs. F_v curves present a discontinuity that corresponds with the monolayer rupture. The threshold F_v value to disrupt the sample depends on the extraction pressure. The higher the surface pressure, the higher the F_v value, so we conclude that, although we do not know if the molecular area of the Langmuir film is the same as in the Langmuir-Blodgett film, we proved that the samples do not relax to reach an equilibrium surface pressure.*

- *LFM proves to be a suitable technique to study the nanotribology of organic monolayers, being sensitive to their molecular structure. Besides, the islands observed at high surface pressures present friction asymmetry, fact that provides information about their structure.*

Tribology Letters Vol 21 No 3 March 2006 (© 2006)
DOI 10 1007 s11249 005-9009 0

Lateral force microscopy study of Langmuir–Blodgett films of a macrocyclic compound

G Oncins[a,b], J Torrent-Burgues[c] and F Sanz[a,b]*

[a]Department of Physical Chemistry Universitat de Barcelona 08028 Barcelona Spain
[b]Center of Nanobioengineering of Catalonia (CREBEC) 08028 Barcelona Spain
[c]Department of Chemical Engineering Universitat Politecnica de Catalunya Colom 1 08222 Terrassa Barcelona Spain

Received 4 October 2005, accepted 19 December 2005, published online 25 April 2006

Langmuir Blodgett films of 4-phenyl 4 sulfide 11 (1 oxodecyl) 1 7-dithia 11-aza-4 phosphacyclotetradecane a thiomacrocyclic compound used as a Cu(II) ions sensor were extracted over mica at several surface pressure values from two subphases pure water and a 0 01 M Cu(II) aqueous solution Atomic Force Microscopy and Force Spectroscopy (Lateral Force Microscopy) were used to study both the morphology and the nanomechanical response of Langmuir-Blodgett films A correlation between extraction pressure and monolayer mechanical properties was observed so an increase in the extraction pressure of the monolayers corresponds with an increase in the vertical force at which the monolayer breaks while doing lateral force experiments Experimental data proves that Langmuir-Blodgett extraction technique truly obtains monolayers with different nanotribological properties as a function of the extraction surface pressure The formation of islands on top of the monolayers was studied and a model mechanism of formation is proposed A higher friction value was measured on the islands than on the monolayer and friction asymmetry was observed in the latest stage of island formation

KEY WORDS Nanotribology friction test methods AFM Langmuir-Blodgett films

1. Introduction

Langmuir Blodgett films (LBs) have been a matter of extensive research during the last decades because of their suitability as models to study molecular organization [1 11] and a wide range of monolayers and multilayers of different molecules have been studied with this technique in the past [12 15] The capability to control either the chemistry of the subphase, the area per molecule and the extraction surface pressure of the layers is an alternative over other preparation techniques of supported monolayers such as Self-Assembled Monolayer deposition (SAMs) [16] The control of the film transfer to the substrate and the possible relaxation of the extraction surface pressure of the supported film over time are still subject to controversy Scanning Probe Microscopies have proved to be suitable to study monolayers at a molecular level [17,18] LBs have been studied using Atomic Force Microscopy (AFM) [8,9,12 13,19] to resolve its morphology and properties Alternatively, Surface Force Apparatus (SFA) has been used to resolve the mechanical properties of these layers at a nanometric level in different media and conditions [20,21]

Lateral Force Microscopy (LFM) has become an increasingly popular technique to study the frictional and nanotribological properties of surfaces [22–25] The development of suitable techniques to calibrate the vertical [26 30] and lateral [31,32] spring constants of the probes used in LFM measurements have allowed to obtain quantitative friction results in the NanoNewton range [23 25] LFM has been used to study the frictional properties of Langmuir–Blodgett layers [33–35], engineering coatings [36], surfaces of Micro-Electro-Mechanical Systems (MEMS) [37,38] and to study organic layers such as thiols on gold [39,40], alkylsilanes on mica [41] or silicon oxide substrates and alkanephosphonates on different crystallographic planes of aluminum [42] The versatility of this technique allows studying the samples under liquid to test phospholipid bilayers on its physiological media [43]

4-Phenyl-4-sulfide-11-(1-oxodecyl)-1,7-dithia-11-aza-4-phosphacyclotetradecane (compound A), figure 1, has a thiomacrocycle that permits to bind copper ions, so acting as a copper ionophore [44,45] A comparison of the mechanical properties of LB films of compound A extracted either from the water subphase or from the Cu(II) aqueous solution subphase offers the opportunity to study the influence of Cu(II) ions in the rheological properties of LBs of compound A

In summary, the aim of the present work is to study the morphology and mechanical properties of LBs formed by compound A using AFM and LFM LBs

*To whom correspondence should be addressed
E mail fsanz@ub edu

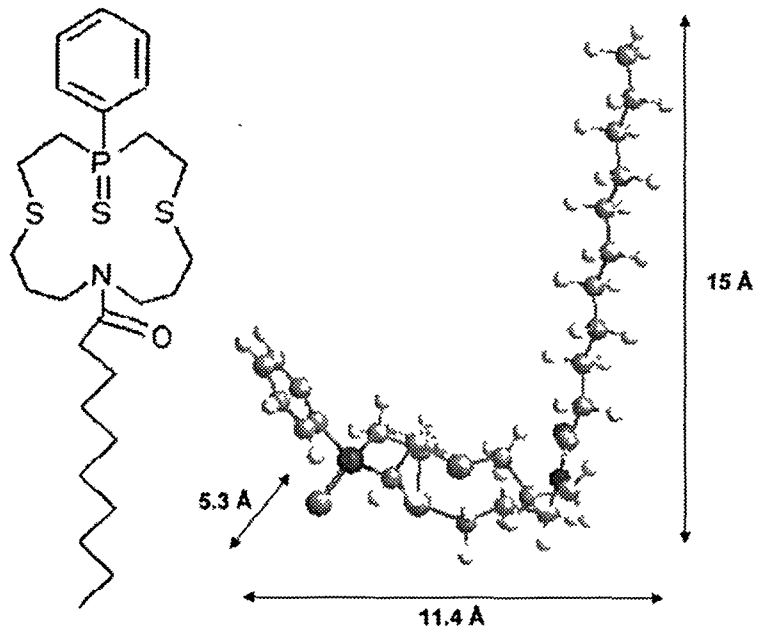

Figure 1. Molecular structure of 4-phenyl-4-sulfide-11-(1-oxodecyl)-1,7-dithia-11-aza-4-phosphacyclotetradecane (compound A).

were extracted at different surface pressures and from the two mentioned subphases, so the change in the nanotribological properties was studied. The correlation between the surface pressure-area isotherms of compound A and the measured lateral force values obtained by LFM on the monolayers give a new insight in the field of nanotribology of LBs.

2. Experimental section

2.1. Langmuir Blodgett films preparation

Langmuir films were obtained in a NIMA 1232D1D2 Langmuir Blodgett trough (area = 1200 cm^2). Pure water (Millipore MilliQ grade), and a 0.01 M solution of $Cu(NO_3)_2$ (analytical grade) were used as subphases. A solution of compound A [46] in chloroform, at a concentration of 1 mg·ml, was spread over the corresponding subphase, and 15 min were lag before measurements in order to permit evaporation of the solvent. The compression speed was 50 cm^2 min.

The corresponding LB films were transferred at constant pressure onto a freshly cleaved atomically flat mica surface. The transfer was done using a NIMA 1232D1 dipper, at several surface pressures and at a constant temperature of 22 °C. The substrates were sheets of 1 cm×1 cm cut from reed mica. LB films were obtained following a Z deposition, that is, the sheet of mica is first introduced in the subphase and once the Langmuir film is formed, the mica sheet is pulled up with an extraction speed of 10 mm/min. The measured transfer ratios were close to 100%.

2.2. AFM and LFM Measurements

All measurements were performed with a Dimension 3100 microscope attached to a Nanoscope IV controller (Digital Instruments, Santa Barbara, CA) in contact mode using V-shaped Si_3N_4 tips (OMCL TR400PSA, Olympus, Japan) with a nominal spring constant of 0.08 N m. Force curves were performed always before acquiring topographic images in order to apply the minimum force on the surface and to avoid any monolayer damage. The instrument was placed on a vibration isolation table and in an isolation box (TMC, Peabody, MA). Temperature was maintained between 19 and 21 °C and humidity was fixed to 40–50% with the aid of a nitrogen flux inside the isolation box.

Vertical spring constant force calibration was performed with a Force Probe1-D MFP (Asylum Research, Santa Barbara, CA). Individual spring constants were calibrated using the thermal noise method [30] after having measured the piezo sensitivity (V/nm) after several minutes of performing force plots to avoid hysteresis.

Lateral force calibration [31] was performed to obtain quantitative friction values, using a wedge silicon oxide

calibration grating (Mikro-Masch TGG01) providing two facets joined at a known dihedral angle Raw data treatment was performed with Matlab scripts provided by R Carpick group [47] Briefly, the scripts were used to generate friction versus load data sets from Nanoscope files For friction versus load measurements an ascending saw tooth waveform from an external function generator (Agilent Palo Alto CA) was subtracted from the vertical photodetector signal obtained through the Signal Access Module (Digital Instruments, Santa Barbara, CA) using a home-made card The resulting voltage was inserted to the vertical photodetector signal through the Signal Access Module allowing the feedback control to maintain a steadily increasing normal force over the course of a friction versus load experiment The lateral motion of the tip was set to 25 nm at 6 1 Hz with 512 lines and 512 pixels per line As a result, a whole friction versus load curve ranging from low loads to high loads was obtained every 84 s We choose to ramp the force from low loads to high loads because we wanted to study the breakage of deposited layers as an increasing force was applied

3. Results and discussion

3 1 Morphology of the monolayers

Figure 2 shows the surface pressure-area per molecule isotherms of compound A on pure water subphase (curve a) and on a 0 01 M Cu(II) aqueous solution subphase (curve b) The change in shape of the isotherms denotes the influence of copper ions present in the subphase Curve a) in figure 2 nearly reaches a plateau at ~12 3 mN m, while curve b) only shows an inflexion point at ~15 5 mN m Arrows in figure 2 indicate the values of the surface pressure at which the LBs were extracted for its characterization

Figure 3 shows the AFM images of compound A LBs extracted from a pure water subphase at surface pressures of 4 (a), 8 (b) 12 (c) and 13 mN m (d) The

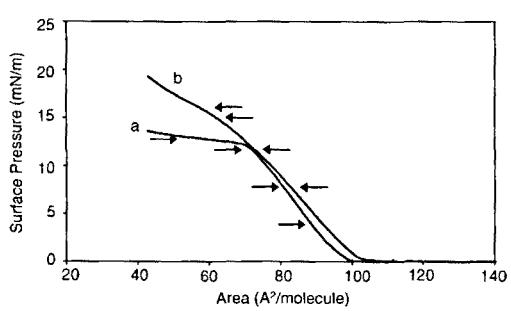

Figure 2 Surface pressure area isotherms of compound A with different aqueous subphases (a) Water (b) 0 01 M Cu(II) aqueous solution The arrows show the extraction pressures studied in the present work

presence of a complete monolayer covering the entire mica surface was verified scratching the surface with the AFM tip at 50 60 nN (images not shown) and measuring the height of the monolayer in the rim of the scratch, being *ca* 1 nm at the minimum vertical force In figure 3, we show the islands of compound A found on top of the monolayer for all the extraction pressures For surface pressures lower than 12 3 mN/m (pressures below the plateau threshold) the height of the islands reached a maximum height of 1 nm and their size increased with increasing extraction pressure For pressures higher than 12 3 mN/m (plateau region in the isotherm), aggregates ~15–17 nm high (figure 3(d)) were formed We were unable to detect any kind of multilayered organization in these aggregates

Figure 4 shows the AFM images of the monolayers extracted from the Cu(II) aqueous solution subphase at 8 (a), 12 (b) and 16 mN/m (c), respectively Islands do not appear below 15 5 mN m, the inflexion point in the isotherm for Cu(II) aqueous solution subphase (figure 2, curve b) For surface pressures higher than this value the aggregates observed on top of the monolayer were ~13–17 nm high (figure 4(c)), very similar to those observed for LBs on water subphase at 13 mN m (figure 3(d)) Correlating the isotherms with AFM images the formation of aggregates seen on water subphase at 13 mN m and on Cu(II) aqueous solution subphase at 16 mN m corresponds with a local collapse of the monolayer, which is due to the asymmetric nature of the compound A molecules and to the lack of a strong hydrophilic group Then, the particular shape of the isotherm is a consequence of the molecular structure of the compound A (figure 1) and its interaction with the subphase High compressions of the monolayer on water subphase lead to the slip out of molecules rather than to changes in the conformation or orientation of the molecules (phase changes) and consequently high surface pressures cannot be reached The effect of Cu(II) ions in the subphase is to bind the compound A molecules and to stabilize the monolayer in some degree As a consequence, the plateau in the isotherms is removed and the corresponding AFM images demonstrate that it is linked to the absence of islands on top of the monolayer for extraction surface pressures below the inflexion point

Compressibility coefficient values (around 25×10^{-3} m mN) calculated for the raising part of the curves a and b of figure 2, indicate the presence of a liquid expanded (LE) phase It has also been corroborated by AFM but with the characteristic that some islands form on top of the monolayer

3 2 Monolayer Friction by LFM

Friction versus load curves were performed on the monolayer on areas free of islands and debris ranging

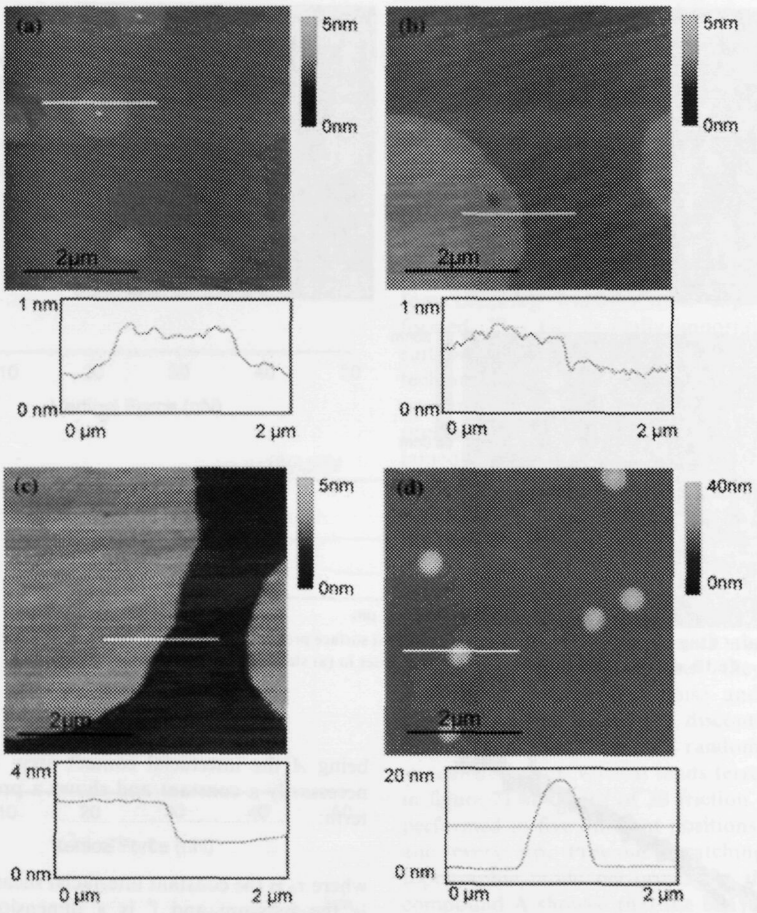

Figure 3. AFM images of Langmuir–Blodgett films extracted at different surface pressures. (a) 4 mN/m, (b) 8 mN/m, (c) 12 mN/m, (d) 13 mN/m. Subphase: water. Images area 5 μm^2. The section corresponds with the white lines on the topography image.

from no-contact to high vertical loads and avoiding the adhesive region (figure 5). Experiments were performed this way to test the response of the Langmuir–Blodgett monolayer of compound A against an increasing vertical load. Preliminary experiments were performed to check friction hysteresis when the load values ranged from low to high values and *vice versa* (figure 5). No hysteresis was detected in the contact region, although there were differences around 0 nN load. In friction versus load curves acquired from low to high load values a nearly 0 nN initial friction regime was observed between tip and monolayer. Having in mind that measurements were performed from no-contact to high vertical loads, this initial regime corresponds with the tip coming into contact with the water layer present on the monolayer (all measurements were performed at 40–50% RH). This low friction initial regime is believed to be due to the slow reaction of the feedback loop as the tip contacts the water layer on the monolayer of compound A. When performing experiments from high loads to no-contact (figure 5, white dots), there is no such a behavior around 0 nN vertical load because the feedback keeps on working until the snap-off event. At 1–2 nN load range, friction increased steeply due to tip and monolayer coming into contact.

We attempted to fit our experimental friction versus load curves on compound A monolayers with several contact mechanics models, namely Johnson–Kendall–Roberts (JKR) [48] and Derjaguin–Müller–Toporov (DMT) [49]. We also attempted to fit our data with the transition equation proposed by Carpick *et al.* [50]. This model permits to adjust a transition parameter (α) that takes values from 0 to 1. When $\alpha = 0$, the equation corresponds to the DMT model and when $\alpha = 1$, it

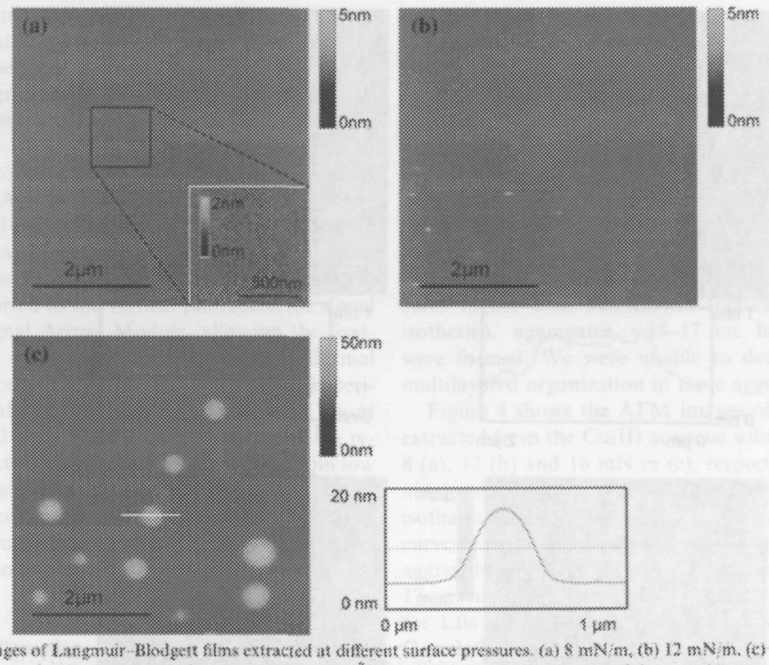

Figure 4. AFM images of Langmuir–Blodgett films extracted at different surface pressures. (a) 8 mN/m, (b) 12 mN/m, (c) 16 mN/m. Subphase: Cu(II) aqueous solution. Images area 5 μm^2. Inset in (a) shows the presence of the monolayer.

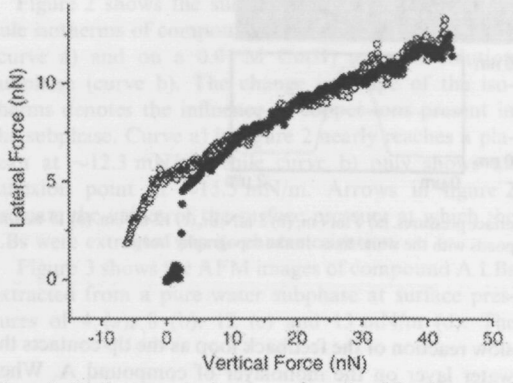

Figure 5. Friction versus load curves performed on LBs of compound A extracted at 12 mN/m with water surface. White curve shows results taken from high loads to low loads and black curve show results taken from low loads to high loads. Each curve is the average of 20 curves performed in five different places on the surface of the monolayer.

corresponds with the JKR model. None of these models was suitable for our measurements. We believe that the main reason is that these contact mechanics models are only valid for homogeneous, isotropic, linear and elastic materials [48]. This is not the case of Langmuir–Blodgett films on mica. Moreover, these models consider that shear strength τ is constant. Friction force (F) for a single asperity is given by [51]:

$$F = \tau \cdot A$$

being A the interfacial contact area. In fact, τ is not necessarily a constant and shows a pressure-dependent term:

$$\tau = \tau_0 + \zeta p$$

where τ_0 is the constant interfacial shear strength term, p is the pressure and ζ is a dimensionless coefficient. Studies concerning friction measurements at the nanoscale have shown that the shear strength can vary depending on the nature of the sample [52]. For all this we believe that these models are not really suitable to explain the contact between an AFM tip and a Langmuir–Blodgett monolayer.

Figure 6 shows friction versus load curves obtained on compound A LBs extracted at several surface pressures. Although the general trend of the curves is roughly the same in all cases, there are some differences that can be related with the extraction pressure and mechanical properties of the monolayers. After the initial contact between tip and monolayer, a region in which the tip frictions the monolayer is reached. This region ends with the appearance of a discontinuity in the friction versus load curve that is marked with an asterisk in figure 6. The load at which this discontinuity appears increases as the monolayer extraction pressure does (8.5 ± 2.3 nN at 8 mN/m, 20.1 ± 2.8 nN at 12 mN/m and 29.5 ± 5.2 nN at 16 mN/m). Previously, we have shown that phospholipid bilayers break under the

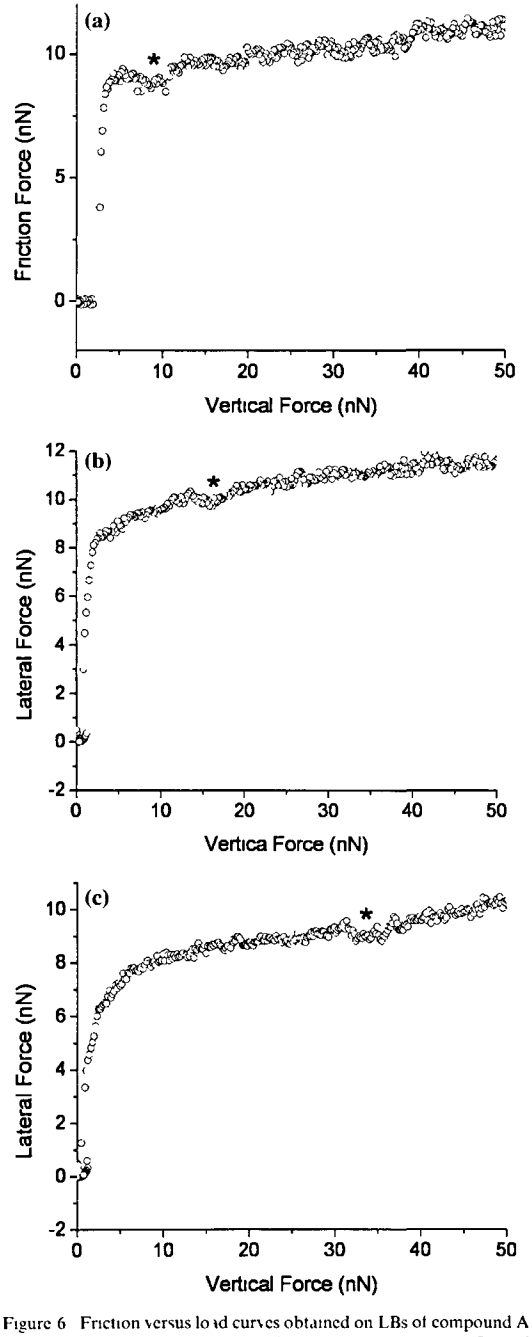

Figure 6 Friction versus load curves obtained on LBs of compound A extracted at different pressures The experiments were performed increasing the vertical load from no-contact to 50 nN Subphase Cu(II) aqueous solution (a) 8 mN m (b) 12 mN m (c) 16 mN m A discontinuity related with the breakage of the monolayer is marked with a * in the graphs

exertion of a certain vertical load and that this load increases as the mechanical strength of the bilayer increases [43,51] This behavior had also been studied with lateral force microscopy and a discontinuity in friction versus load curves had been detected and related with the break of the phospholipid bilayer [43] So, the discontinuities in the friction versus load curves obtained on compound A monolayers correspond well with their breakage As a consequence, the presence of this discontinuity is a way to measure the vertical force that the monolayer withstands before breaking while friction experiments are performed This fact is really important to confirm the suitability of the Langmuir-Blodgett extraction technique to get layers with different nanotribological properties as a function of the extraction surface pressure To ensure the reproducibility of the obtained results, friction versus load experiments were performed with two different calibrated tips and in several experiments The results are shown in figure 7(a) The magnitude depicted is the vertical force at which the LB broke as friction versus load experiments were performed Random discontinuities were detected in friction versus load curves besides the ones that correspond with the rupture of the monolayer We believe that they correspond to mechanical or electrical noise and they appear at random vertical loads The discontinuities presented in figures 6 and 7 are not random at all and they appear at certain vertical loads (error bars are shown in figure 7) in 20 out of 30 friction versus load loops performed in five different positions for every sample and every tip Previous scratching experiments in topographic mode performed on the monolayers of compound A showed that the bilayer can be removed from the surface of the mica applying loads in the range of vertical forces shown in figure 7

The friction coefficient on the monolayer (the slope of the linear region of contact between tip and monolayer in the friction versus load curve) at an extraction pressure of 16 mN m was calculated to be $0\,124 \pm 0\,002$ For vertical load values higher than that corresponding with the discontinuity shown in the friction versus load curves, there is a linear region with a friction coefficient that was calculated to be $0\,140 \pm 0\,002$ This friction coefficient is quite similar to the friction coefficient obtained on mica under the same parametric conditions ($0\,142 \pm 0\,001$), so this region corresponds to the contact between the tip and the monolayer supporting substrate (mica) This fact has also been reported in a previous work [53]

To compare the mechanical properties of layers extracted from the two subphases, experiments have also been performed on monolayers extracted in pure water subphase Results are shown in figure 7(b) The columns

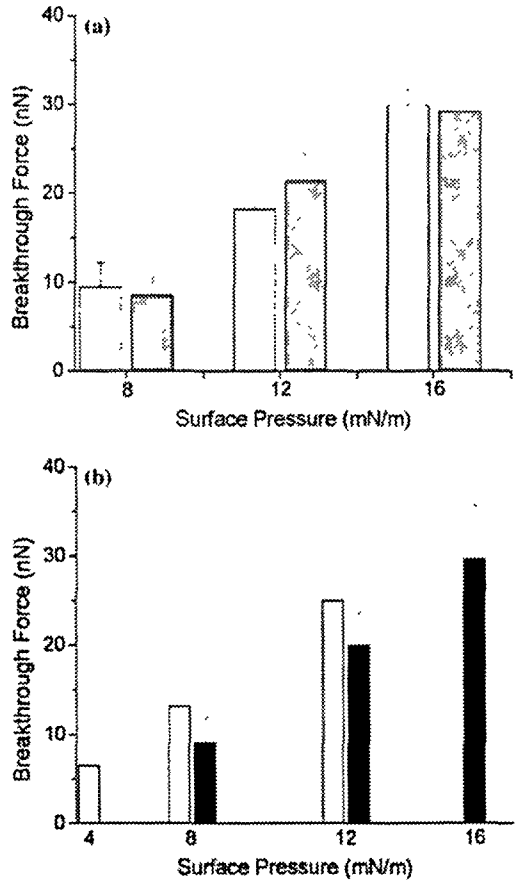

Figure 7. Averages of the vertical breakthrough forces obtained in the friction versus load experiments. (a) White and grey columns stand for experiments performed on LBs extracted with Cu(II) ions in the subphase in two different days with two different calibrated tips. Error bars stand for standard deviation. Every column is the mean value of 20 friction versus load experiments obtained in five different locations on the surface. (b) Comparison between breakthrough forces obtained from friction versus load data on LBs extracted with different subphases. White columns: water subphase. Black columns: Cu(II) aqueous solution subphase.

show the vertical force at which the break appears in the friction versus load curves, being the feature more directly related with the mechanical resistance of compound A monolayers. The discontinuity (breakage of the monolayer) also shifted to higher load as the extraction pressure increased. White columns show the results obtained on monolayers extracted with water subphase and black columns correspond with monolayers extracted with Cu(II) aqueous solution subphase. Interestingly, when monolayers with water and Cu subphase were extracted at the same pressure (8 and 12 mN/m), the break appeared at higher loads in water subphase. As can be seen in figure 2, the area/molecule to get a certain surface pressure is higher in Cu(II) aqueous solution subphase than in water subphase. This means that, to reach a certain surface pressure, molecules are more packed with a water subphase that with a Cu subphase. In conclusion, the discontinuity observed in the friction versus load curves is more sensitive to the area/molecule that to surface pressure. As a consequence, as the area/molecule decreases, the load at which the monolayer breaks in friction versus load curves increases.

3.3. Formation of islands and friction asymmetry

Friction asymmetry is an effect that has been detected in a number of previous works concerning thiolipid Langmuir Blodgett monolayers [54], polydiacetylene monolayers [55] and monoglycerol monolayers [35] and that consists in a different friction response depending on the scanning direction. As a consequence, trace and retrace friction signals show different value. This asymmetry was reported to be due to the orientation of the molecules on the surface [49,50]. In these works, friction changes as a function of the molecule hydrocarbon backbone orientation and tilting. Compound A

molecule has also a carbonated backbone, although the molecule is highly asymmetric. We have observed a 15–20% of friction asymmetry only on islands onto compound A monolayer (figure 8). As it has been shown in figure 3, islands up to 1 nm high appear on top of monolayers at pressures up to 12 mN/m. In fact, these islands show heights around 0.3 nm or 1 nm, this last value corresponding with the height of the monolayer on mica. This two height regimes are shown in the AFM image in figure 8(c). The island in the upper-right corner of the image is 1 nm high while the island in the lower-left corner is 0.3 nm high. The latest is difficult to detect topographically but it is nicely shown in the friction image (figure 8(d)). Interestingly, friction asymmetry only appears on the islands that are 1 nm high and not in the islands that are 0.3 nm high. We have attributed the existence of the two kinds of islands to two different consecutive formation steps that have been depicted in figure 9. We suggest the possibility of local surface pressure fluctuations and the asymmetric nature of compound A being responsible for the formation of these islands on monolayers extracted with water subphase. The lack of strong hydrophilic centers in the thiomacrocycle leads to a weak interaction between compound A and the water subphase. As a consequence, it seems possible to think that compound A molecules can be locally pushed up (figure 9(a)) forming an aggregate on the surface (figure 9(b)). These aggregates can be seen in the center of the islands shown in figure 3(a) (two islands in the upper part of the image) and in figure 8(c) (island in the upper-right corner of the image). Lately, these aggregates spread forming a circular island that is 0.3 nm high (figure 8(c), lower part of the image and figure 3(a)). Sometimes, the accumulation of molecule A and the disordered islands coexist (as the aggregate disappears, the disordered island grows). Finally, the disordered islands increase their packing density and reach a height of 1 nm (island in figure 3(c)), which is the height of the monolayer on mica. On the other hand, when there are Cu(II) ions in the subphase there are no islands on top of the monolayer until a pressure of 15.5 mN/m is reached. So it is clear that Cu(II) ions play an important role in the morphology of the monolayer. We think that low height islands correspond with the first stage of island formation (figure 9(c), first step after molecules of compound A have been expelled from the monolayer), where molecules are disordered. Under further compression,

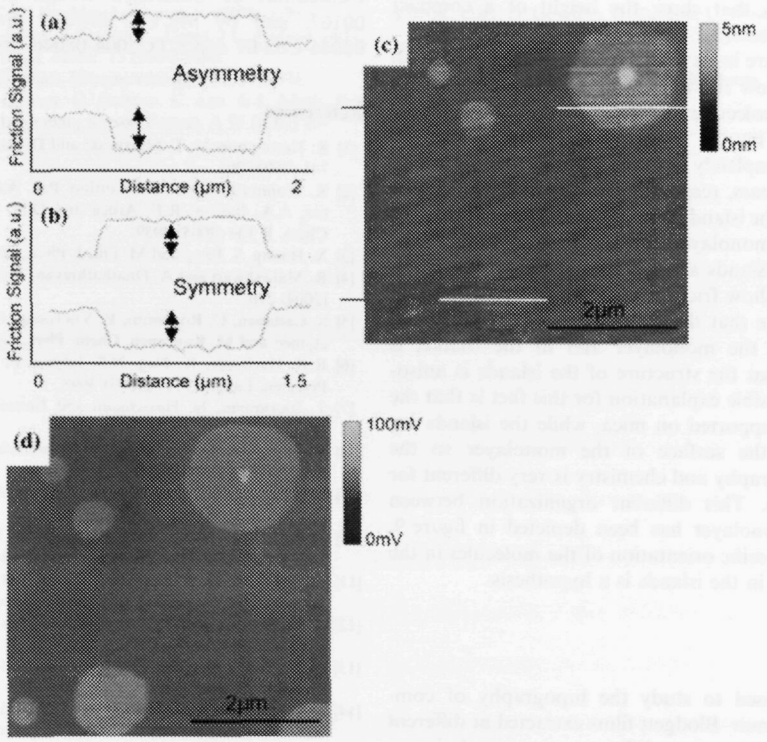

Figure 8. Friction loops obtained on islands on compound A monolayer extracted on water subphase at 8 mN/m. (a) Friction signal of an island completely formed, showing an asymmetric friction. (b) Island in formation process showing symmetric friction. (c) Topographic image of the monolayer. (d) Friction image of the monolayer (trace—retrace friction signal).

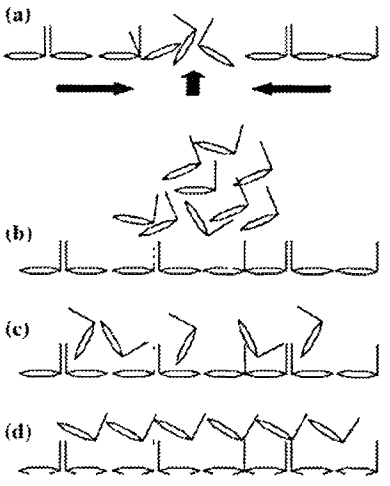

Figure 9. Different stages in the formation of an island on a compound A LB film. (a) Expulsion of molecules from the monolayer. (b) Formation of an aggregate on the monolayer. (c) Spreading of the aggregate to form a disordered island on the surface of the monolayer. (d) Ordering of the island on the monolayer under further compression.

these molecules rearrange and order on the monolayer to form islands that show the height of a compact monolayer (figure 9(d)).

Islands that are in its first stage of formation (0.3 nm high) do not show friction asymmetry because there is not a regular molecular order, so the friction signal is not influenced by the scanning direction. When the islands are completely formed (1 nm high islands), asymmetry appears, responding to the molecular order established on the island. It is interesting to note that the friction of the monolayer and the friction of the completely formed islands are different and that the monolayer does not show friction asymmetry. From this fact we can conclude that the way compound A molecules are ordered in the monolayer and in the islands is different and that the structure of the islands is anisotropic. One possible explanation for this fact is that the monolayer is supported on mica, while the islands are supported on the surface of the monolayer so the substrate topography and chemistry is very different for both structures. This different organization between islands and monolayer has been depicted in figure 9, although the specific orientation of the molecules in the monolayer and in the islands is a hypothesis.

4. Conclusions

AFM was used to study the topography of compound A Langmuir Blodgett films extracted at different surface pressures from two different aqueous subphases. The formation of islands on the monolayer from the pure water subphase was analyzed and a model for its formation was proposed. Cu(II) ions effect on the compound A monolayer is evident in the isotherms and in AFM images, and these ions increase the stability of the monolayer. LFM has proved to be useful to study the nanotribology of compound A-like films. The breakage of the LB monolayers was detected as a discontinuity in the friction versus load curves. In both cases, for pure water and for Cu(II) aqueous solution subphases, there is a shift of the monolayer breakage load towards higher values as the extraction pressure increases. Besides, an asymmetry in friction was observed for compound A islands in the latest stage of formation and this effect was related with its arrangement in the LB films.

Acknowledgments

The authors thank Dr. A. Errachid and group of Prof. J. Casabó for kindly providing the compound A. G.O. thanks Matt Brukman and Robert Carpick (University of Wisconsin, WI) for providing the Matlab scripts to analyze friction data and Samuel Lesko (Digital Instruments) and Marc Castellarnau (University of Barcelona) for helping in the development of the experimental setup. This work has been supported by Generalitat de Catalunya trough project 2002PIRA 00167, and by MCYT through projects CTQ2004-08046-C02-01 and CTQ2004-08046-C02-02.

References

[1] R. Hermanowski, T. Martyński and D. Bauman, J. Mol. Struct. 741 (2005) 201.
[2] K. Wohnrath, C.J.L. Constantino, P.A. Antunes, P.M. dos Santos, V.A. Batista, R.F. Aroca and O.N. Oliveira Jr., J. Phys. Chem. B 109 (2005) 4959.
[3] X. Huang, S. Jiang and M. Liu, J. Phys. Chem. B 109 (2005) 114.
[4] R. Maheshwari and A. Dhathathreyan, J. Colloid Interf. Sci. 275 (2004) 279.
[5] S. Cattaneo, C. Rochenito, E. Vuorimaa, A. Efimov, H. Lemmetyinen and M. Kauranen, Chem. Phys. Lett. 377 (2003) 306.
[6] R.R. Harbottle, K. Nag, N.S. Intyre, T. Possmayer and N.O. Petersen, Langmuir 19 (2003) 3698.
[7] T. Bromholm, N. Hvissenkim and Reitzel, J. Mater. Chem. 9 (1999) 1975.
[8] S. Leporatti, E. Bruzgeru, G. Brzezinski and H. Mohwald, Langmuir 14 (1998) 7503.
[9] S. Leporatti, G. Brezesinski and H. Möhwald, Colloid Surf. A 161 (2000) 159.
[10] M.K. Sanyal, M.K. Mukhopadhyay, M. Mukherjee, A. Datta, J.K. Basu and J. Penfold, Phys. Rev. B 65(3) (2002) 033409-1.
[11] D.Y. Takamoto, E. Aydil, J.A. Zasadzinski, A.T. Ivanova, D.K. Schwartz, T. Yang and P.S. Cremer, Science 293 (2001) 1292.
[12] A. Ulman, *An Introduction to Ultrathin Organic Films* (Academic Press, Boston, 1990).
[13] M.C. Petty, *Langmuir–Blodgett Films, An Introduction* (Cambridge University Press, Cambridge, 1996) ch. 3.
[14] K.J. Stine and B.G. Moore, in *Nanosurface Chemistry*, ed. M. Rosoff (Marcel Dekker Inc., New York, 2002).
[15] T.H. Richardson, in *Functional Organic and Polymeric Materials*, ed. T.H. Richardson (John Wiley and Sons, Ltd., Chichester, 2002) ch. 5.

[16] S H Gyepi-Garbrah and R Sulerova Phys Chem 4(14) (2002) 3436
[17] X Xiao, G Liu, D H Charych and M Salmeron, Langmuir 11 (1995) 1600
[18] J T Woodward and D K Schwartz, J Am Chem Soc 118(33) (1996) 7861
[19] Y F Dufrêne and G U Lee, BBA Biomembranes 1509 (2000) 14
[20] J Schneider P Berndt, K Hiverstick S Kumar, S Chiruvolu and M Tirrell Langmuir 18(10) (2002) 3923
[21] K Kurihara Hyomen Kagaku 18(19) (1997) 618
[22] G J Leggett, Anal Chim Acta 479 (2003) 17
[23] R W Carpick and M Salmeron Chem Rev 97 (1997) 1163
[24] B Bhushan, J N Israelachvili and U Landman, Nature 374 (1995) 607
[25] J Krim Surf Sci 500 (2002) 741
[26] C P Green H Lioe, J P Cleveland, R Proksch, P Mulvaney and J E Sader Rev Sci Instr 75(6) (2004) 1988
[27] J L Sader Rev Sci Instrum 66(9) (1995) 4583
[28] J P Cleveland and S Manne Rev Sci Instrum 64(2) (1993) 403
[29] J L Hutter and J Bechhoefer, Rev Sci Instrum 64(7) (1993) 1868
[30] E L Florin M Rief, H Lehmann M Ludwig C Dornmair, V T Moy and H E Gaub, Biosens Bioelectron 10 (1995) 895
[31] D F Ogletree, R W Carpick and M Salmeron Rev Sci Instrum 67(9) (1996) 3298
[32] R G Cain, M G Reitsma S Biggs and N W Page, Rev Sci Instrum 72(8) (2001) 3304
[33] R W Carpick D Y Sasaki and A R Burns Tribol Lett 7 (1999) 79
[34] U Gehlert, J Fang and C M Knobler J Phys Chem B 102 (1998) 2614
[35] K Hisada and C M Knobler, Langmuir 16 (2000) 9390
[36] C Corbella, M Vives G Oncins, C Canal J L Andujar and E Bertran Diam Relat Mater 13 (2004) 1494
[37] H Liu and B Bhushan Ultramicroscopy 97 (2003) 321
[38] W R Ashurst C Yau C Carraro C Lee G J Kluth R T Howe and R Maboudian, Sensor Actuat A 91 (2001) 239
[39] N J Brewer B D Beake and G J Leggett, Langmuir, 17 (2001) 1970
[40] L Li, S Chen and S Jiang Langmuir 19 (2003) 666
[41] E Barrena S Kopta, D F Ogletree D H Charych and M Salmeron, Phys Rev Lett 82(14) (1999) 2880
[42] M J Brukman, G Oncins T D Dunbar, L D Boardman and R W Carpick, Langmuir (in press)
[43] G Oncins S Garcia-Manyes and F Sanz, Langmuir 21(16) (2005) 7373
[44] I A Marques de Oliveira, M Pla-Roca L Escriche, J Casabo, N Zine, J Bausells, F Bessueille, J Samitier and A Errachid *2004 IEEE Sensors 2004 The 3rd IEEE Conference on Sensors*, Vienna Austria (2004)
[45] I A Marques de Oliveira M Pla-Roca L Escriche J Casabo N Zine, J Bausells, J Samitier and A Errachid Mat Sci Eng C (in press)
[46] J Torrent-Burgues, M Pla Ll Escriche J Casabo, A Errachid and F Sanz, Colloid Surface A (submitted)
[47] The scripts are available for non commercial use at http mandm engr wisc edu faculty_pages_carpick toolbox htm
[48] K L Johnson K Kendall and A D Roberts Proc Roy Soc Lond A 324 (1971) 301
[49] B V Derjaguin V M Muller and Y P Toporov, J Colloid Interface Sci 53 (1975) 314
[50] R W Carpick, D F Ogletree and M Salmeron, J Colloid Interface Sci 211 (1999) 395
[51] J X-D Hu Xiao, D F Ogletree and M Salmeron Surf Sci 327 (1995) 358
[52] O Pietrement and M Troyon, Langmuir 17 (2001) 6540
[53] S Garcia Manyes, G Oncins and F Sanz, Biophys J 89(3) (2005) 1812
[54] M Liley D Gourdon D Stamou, U Meseth T M Fischer C Lautz, H Stahlberg H Vogel N A Burnham and C Duschl Science 280 (1998) 273
[55] R W Carpick D Y Sasaki and A R Burns, Tribol Lett 7 (1999) 79

Chapter 5

5.Biological coatings. The nanobio revolution.

5.1 INTRODUCTION

As we have seen, there are several ways to reduce friction in MEMS and NEMS: we can coat them with hard films as is the case of DLC or we can also functionalize their surface with alkanethiols, fatty acids, phosphonic acids or even alkanesilanes in an attempt to reduce the coating thickness and to take advantage of the possibility of chemical functionalization so as to meet specific mechanical requirements. Nevertheless, we can also be interested in functionalizing our devices with complex biological structures as proteins in order, for example, to use them inside our body[148,260]. The union between the electronics industry and the biological sciences has been for a long time an issue only dealt with in science-fiction movies but nowadays great efforts are being done to integrate both worlds[261-265]. It is remarkable the report released by Castellana et al.[266], where phospholipid membranes integrated in sensor devices by means of photolithographic, micro-contact printing and related techniques are reviewed. In this regard, an interesting sensor device was developed by Gu et al.[267], who were able to detect the conductivity change induced in a membrane by a certain analyte when it binds to a transmembrane protein embedded in the phospholipid bilayer. A schematic of the device is depicted in Fig. 30.

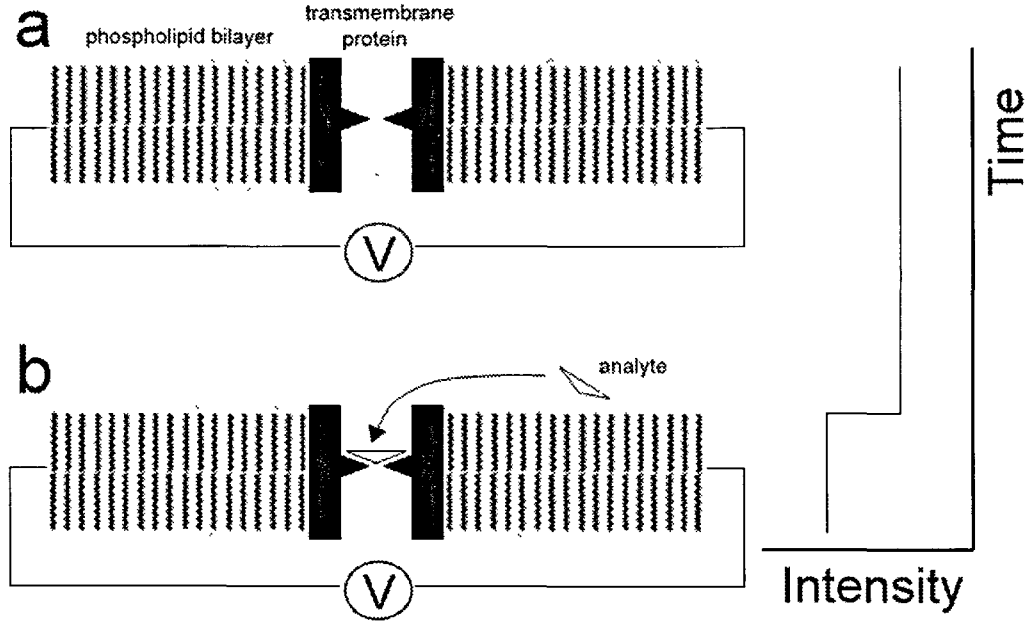

Fig. 30. Example of BioMEMS. Transmembrane proteins embedded in phospholipid bilayers can be used as organic sensors. The presence of the analyte in the channel created by the protein changes the membrane conductivity, which can be recorded and related with the analyte concentration. The detection limits are extremely small, as intensity variations are in the pA range. A similar device was implemented by Gu et al[267].

5.2 WHY PHOSPHOLIPIDS?

In this new and exciting scenario, phospholipid bilayers seem to be the building blocks of the bio-devices coating, as they are used as a support to insert more complex (and potentially interesting) molecules as trans membrane and peripheral proteins or/and receptors. Phospholipid are the main constituent of cellular membranes[268], which are amazing structures in terms of nanotribology and nanomechanics[269], as their rigidity and elasticity can be modulated depending on the physicochemical properties of the medium or on the presence of other intercalated lipids as ergosterol[270] or cholesterol[271]. Then, studying the nanomechanics of phospholipid monolayers and bilayers is mandatory in order to leap towards the integration of biology with MEMS and NEMS. Besides, the complexity of these biological membranes makes of them ideal models to study and isolate the effect of the different interactions that keep molecules together, that is,

van der Waals, hydration and electrostatic forces and that are of relevance in 2-dimensional structures.

Our goal is to study phospholipid membranes from a fundamental point of view, testing their mechanical resistance to be punctured or frictioned by an AFM tip in liquid environment as a function of the ionic strength of the solution (*I*), the temperature and the pH. Of course, this is an ambitious project and although our contribution may be small, it sheds some light that will hopefully help to unveil the mysteries of the nanoworld.

5.2.1 Phospholipid bilayers structure and formation

The membranes of mammalian cells[272] have been designed to provide a semi-permeable barrier able to maintain different aqueous media in each one of their sides (different concentration of ions or biomolecules) and also an electrical potential difference[273]. Besides, the membrane also works as a scaffolding to hold the whole cellular structure so it must retain certain mechanical rigidity[274], although it must be fluid enough to permit the bidimensional diffusion of membrane proteins along its structure[275]. As usual, Evolution has done a superb selection job.

Phospholipids are amphiphilic molecules, that is, they have got two differentiated regions with opposed affinity for water as it can be seen in Fig. 31. To begin with, they present a polar region or headgroup (phosphatidylcholine, phosphatidylethanolamine, phosphatidylserine, etc) that can be charged or zwitterionic, that is, overall neutral but with charge separation. This is the case of phosphatidylcholines (PCs), a phospholipid family named after their polar headgroup that will be discussed more extensively in this thesis, as the vast majority of studies have been performed with them. Besides to the existence of electrical charges, the polar region is hydrophilic, so it dissolves well in water. The apolar region is constituted by two hydrocarbon chains attached to the polar headgroup and that can show a variable unsaturation degree. As you may expect because of its composition, this region is highly hydrophobic, so phospholipid

molecules can partially dissolve depending on the group they show to the liquid medium. When they are in aqueous solution, they tend to form monolayers on the liquid surface with the polar heads towards the liquid and the chains towards the air as depicted in Fig. 32*a*. When the surface of the liquid is saturated, the next option is to dissolve and they do it forming bilayers with the polar heads in the outer part while the hydrophobic chains remain in the core of the bilayer, far from the water medium and responding to the named hydrophobic effect. Instantaneously, the bilayer folds forming spherical units called liposomes (Fig. 32*a*), which are fully stable in solution. These liposomes can regain the planar bilayer structure if they interact with a surface, forming the so-called Supported Planar Bilayers (SPBs), which are depicted in Fig. 32*d*. Obviously, for this process to take place the interaction between the polar heads and the substrate must be more favorable than the interaction between polar heads and water, so electrostatic charges tend to take the Lion's share (Fig. 32*b* and *c*). In the case of PCs, the outer part of the bilayer is positively charged (choline), so PC liposomes easily spread on negative hydrophilic surfaces such as mica but it does not spread on hydrophobic neutral surfaces such as highly ordered pyrolytic graphite (HOPG)[276]. Nevertheless, as we will see in forthcoming sections, the solution pH and the presence of ions can alter the distribution of charges both in the phospholipids and the surfaces, modifying their interactions and, therefore, the quality of the SPBs.

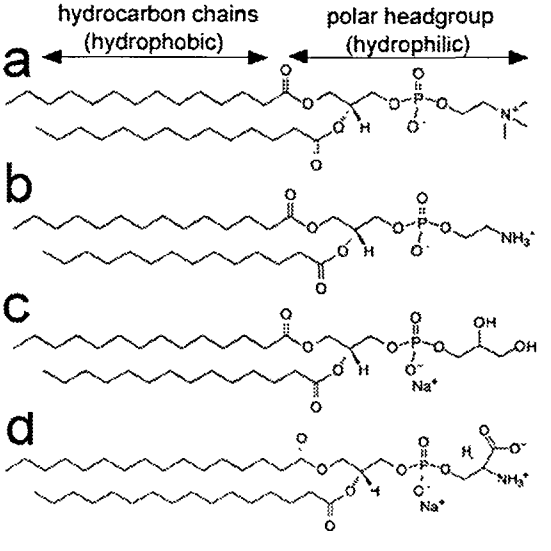

Fig. 31. Several phospholipids with different polar heads and different charges. a) 1,2-Dimyristoyl -sn-Glycero-3- Phosphocholine (DMPC). b) 1,2-Dimyristoyl- sn-Glycero-3-Phosphoethanolamine (DMPE). c) 1,2-Dimyristoyl -sn-Glycero-3- [Phospho-rac-(1-glycerol)] (Sodium Salt) (DMPG) d) 1,2-Dipalmitoyl -sn-Glycero-3- [Phospho-L-Serine] (Sodium Salt) (DPPS). More information in www.avantilipids.com

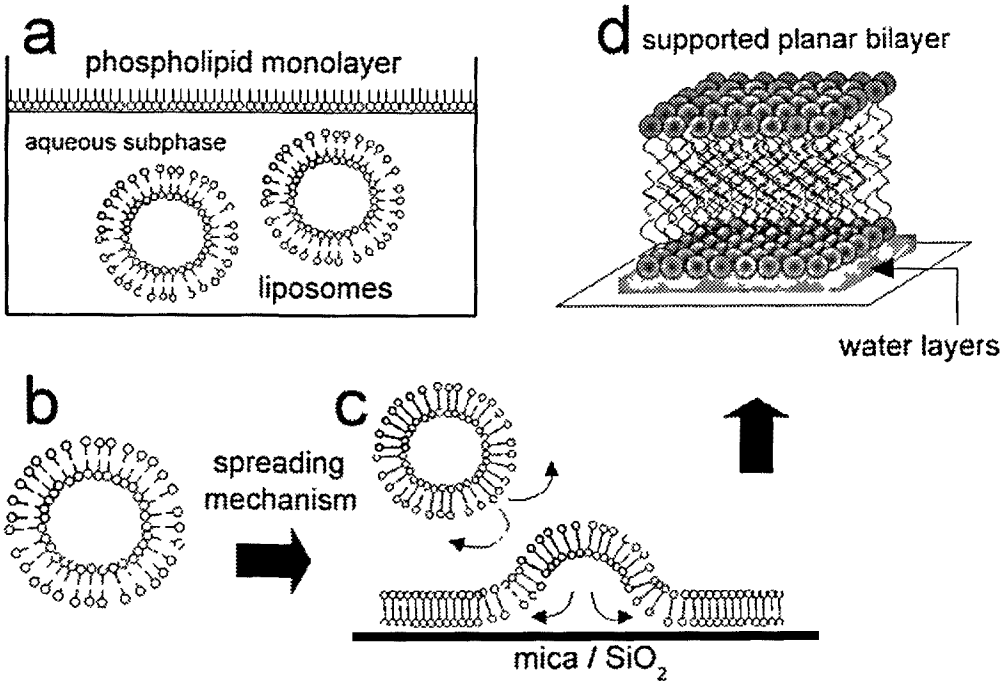

Fig. 32. Supported planar bilayers formation mechanism. a) In solution, phospholipid molecules tend to form a monolayer on the aqueous surface with the polar heads in contact with the liquid. The rest of the molecules form liposomes, hiding the hydrocarbon chains in the hydrophobic core. b) and c) The liposomes can spread on hydrophilic surfaces, forming supported planar bilayers (SPBs). d) Between the substrate and the SPB, there is a certain quantity of water, as both the substrate and the polar heads are hydrophilic.

5.2.1.1 Van der Waals interactions

Van der Waals interactions arise from the proximity between the hydrocarbon chains of adjacent phospholipids molecules and can be calculated as follows[277]

$$E_{VdW} = \frac{3\alpha_0^2 h\nu}{4(4\pi\varepsilon_0)^2}\left[\frac{6}{\sigma^2} + \frac{12}{\left[\sigma^2 + l^2\right]^3} + \frac{12}{\left[\sigma^2 + (2l)^2\right]^3} + \ldots\right]\frac{N_A}{2} \qquad (29)$$

being α_o the polarizability, ε_o the vacuum permittivity, σ the distance between 2 equivalent -CH_2 groups in adjacent molecules, l the distance between consecutive -CH_2 groups in the same hydrocarbon chain and N_A Avogadro's number. For tightly packed hydrocarbon chains, which corresponds to an σ = 0.4 nm (diameter of a hydrocarbon chain), E_{VdW} ~7kJ/mol per -CH_2 group (the total E_{VdW} is obtained multiplying 7 kJ/mol per the number of -CH_2 groups in the molecule). In the case of phospholipids, each molecule is composed of two chains and considering a hexagonal molecular packing[278,279] and a certain σ value, the E_{VdW} for the entire phospholipid bilayer can be calculated as in section 5.4.6. In that case, as the monolayer was a LB film, the surface pressure was controlled and an experimentally controlled σ value was used, obtaining a total E_{VdW} = 19.4 kJ/mol. Considering that the DPPC hydrocarbon chains have 16 carbon atoms, we can see that the packing is not as efficient as in the case of single chain molecules, which have a higher ordering degree. Why nature has chosen two chain molecules when one chain molecules could pack tighter? Perhaps it was thinking about increasing membrane fluidity...

5.2.1.2 Hydration forces

Water plays a key role in the structure of biological membranes, as it mediates the interaction between membranes and contributes to the transport of biomolecules and other substances across phospholipid bilayers. Because of that, the water that surrounds biomembranes has been thoroughly studied, both experimentally and by means of computer simulations. Between the experimental techniques, X-ray and neutron scattering are useful to study the membrane structural changes and the relative position of water[280], while NMR spectroscopy can shed light on the dynamics of these processes and quantify water residence times[281,282]. The hydrogen bonds can be assessed by means of infrared spectroscopy and fluorescence spectroscopy is helpful to study the hydration shells around the phospholipid bilayers and also the dynamics of water[283]. A first point of contact with these experimental techniques can be the review written by Milhaud et al.[284], while simulation studies are reviewed by Berkowitz et al.[285]

Concerning the water-phospholipid interactions, the first question is to answer how water structures around the phospholipid polar headgroups. This issue was studied by Aman et al.[286], who compared his simulations with experimental NMR results and concluded that each DPPC headgroup perturbs ca. 17 water molecules. Besides, they classified the water molecules in two groups depending on the orientation of their dipoles, which can be parallel or perpendicular to the bilayer plane. The results of those authors suggested that water can penetrate the polar headgroup up to a certain extent and that the probability to find a water molecule increased in a sigmoidal way from the inner part of the polar headgroup to the interface liquid-bilayer surface. Nevertheless, these results suggested that the water was not ordered around the polar headgroups, phenomenon that had been previously confirmed experimentally. This contradiction was solved by Pandit et al.[287], who considered the roughness of the bilayer as a key parameter in the calculations and predicted that the headgroups could perturb up to 20 water molecules, obtaining similar results to those reported by Aman[286]. Posterior simulations increased the number of perturbed water molecules up to 25, more in line with experimental calorimetric results[288] and the inner structure of these waters as a function of the distance from the center of the bilayer was resolved. Then, four water layers were identified corresponding with the water inside the monolayer (able to penetrate up to the ester groups), the first and second hydration shell and the bulk water. The first hydration layer has the width of a water molecule, while the secondary layer is thicker, confirming that the higher the distance from the polar headgroup, the less ordered the water molecules are. It is interesting to note that the inner molecules of water have a higher density than those in the bulk, phenomenon that can be explained in terms of the water reorganization around the headgroup electric charges.

Pasenkiewitz-Gierula et al.[289,290] performed the first simulations concerning the formation of hydrogen bonds between water molecules and phospholipid headgroups choosing the specific case of cholines, but it was Lopez et al.[291] who, refining these measurements, reached important conclusions: the carbonyl oxygen

atoms have a better chance of forming hydrogen bonds with water than the ester ones, while the oxygen atoms in the phosphate group are the ones with a better chance as they are closer to the bilayer-liquid medium interface and, consequently, more exposed to water molecules. Moreover, the simulation was able to discriminate between the different oxygen atoms bonded to phosphorus atoms, attributing a hydrogen bond creation probability of 74% for oxygen atoms double bonded to phosphorus atoms (the probability was ca. 20% for single bonded oxygen atoms). The distribution of water molecules around the choline group results in two solvation shells, while the phosphate group is predominantly solvated by water molecules close to the single bonded oxygen atoms. Interestingly, the presence of water molecules bridging other water molecules that solvate the phosphate groups was detected and considered to be, besides electrostatic and hydrogen bonding forces, key interactions to understand the structure and mechanical behavior of the membranes.

Concerning the diffusion of the water molecules that form hydrogen bonds with the phospholipids, it was reported that it is higher for water molecules that are linked to double bonded oxygen atoms, reaching values ca. 2.0×10^{-7} cm^2/s, two orders of magnitude below the diffusion rate of bulk water.

5.2.1.3 Electrostatic forces.

Biomembranes are in contact with electrolytic solutions and are highly influenced by them[292,293], mainly due to the presence of charged groups in the phospholipid polar regions. This charge can interact with water molecules and orient them into different solvation layers as seen in the previous section but it can also interact with ions forming electrostatically bounded phospholipid networks that can be tested, among other techniques, by zeta-potential measurements[294-296] (phospholipids in solution) or by AFM and Force Spectroscopy[297] (for supported conFig.tions, as SPBs or LB films).

A convenient experimental approach to prove the importance of ions in the structure of biomembranes was presented by Egawa et al.[298] These authors studied

the spreading of PC and phosphatidylethanolamine (PE) liposomes onto the mica surface by means of topographic AFM and they found that PCs form bilayers more easily in the presence of $MgCl_2$, while PE phospholipids tend to form double bilayers. They proposed that the PC headgroups, despite being neutral, have a certain negative charge due to some acidic impurities[299]. Also PC bilayers do not spread easily onto the negatively charged mica surface due to electrostatic repulsion. Nevertheless, the ions in solution are able to shield the electrostatic charge both on the mica and on the liposomes surface, promoting the bilayer deposition. Additionaly, they measured the surface potential of the liposomes in solution as a function of the NaCl concentration, reporting a potential increase for PC and PE molecules and also for the mica surface, confirming that ions bind to the phospholipid polar headgroups changing their surface charge. Garcia-Manyes et al. established a relationship between the quality of the monolayers and the zeta-potential of DMPC bilayers, confirming that the adherence of the phospholipids to a surface is extremely dependent on the surface charge of both the bilayer and the substrate[276].

One of the first experimental proves of the structural changes induced in phospholipid structures by ions was observed by Yamaguchi et al.[300] They reported that a 10 mM KCl solution resulted in a reduction of PC phospholipids area per molecule (up to the 90% of the initial area) while the same concentration of $CaCl_2$ produced an enhanced effect (80% of the initial area). They attributed this reduction in area to a closer molecular packing between phospholipids, which is promoted by the electrical shielding of the headgroup charges. In this direction, Makino et al.[301] observed that the tilting of the polar headgroups was dependent on the medium *I* value: at low *I* values, the phosphatidyl groups of DPPC molecules are in the outer part of the bilayer, which mean that the polar headgroups are bended towards the bilayer core as shown in Fig. 33*a*. Nevertheless, as the quantity of ions in solution increases, the heads unfold and the phospholipids pack more efficiently (Fig. 33*b* and *c*). Besides, this orientation change contributes to the zeta-potential variation

observed as a function of *I* value. Interestingly, this work points out that the unfolding process is dependent on the *I* value, but also on the kind of ions[302].

Pandit et al.[303] went a step further, trying to respond some key questions: 1) where in the headgroup do ions bind?; and 2) how many lipids are involved in the lipid-ion complex? By means of simulations of hydrated DPPC bilayers in pure water and in NaCl solution, they concluded that NaCl presence improves the headgroup interaction but also the hydrocarbon chains packing, promoting a bilayer thickness increment of ca. 0.22 nm, which is consistent with the headgroup unfolding model proposed by Makino[301] and depicted in Fig. 33. Nevertheless, Pandit did not observe any change in the headgroup tilting as NaCl is added to the solution. Interestingly, they reported that Na^+ penetrates the polar moiety up to the phosphate group and that each Na^+ ion can coordinate with two of them, while Cl^- accumulates near the choline groups. During these rearrangement processes, the Na^+ ions lose 3-4 water molecules from their first coordination cell, while Cl^-, with its lowest coordination degree, only loses 1 water molecule. Böckmann et al.[304] confirmed the results reported by Pandit, pointing out to the fact that Na^+ can coordinate up to 3 PC carbonyl oxygen atoms (Fig. 34) and extended their studies also to divalent cations. It must be emphasized that experimental measurements concerning the effect of divalent cations on phospholipid bilayers support the existence of orientation changes in the polar moieties as a function of cationic concentration, as demonstrated by NMR experiments concerning DPPC bilayers and $CaCl_2$[305,306]. As you may expect from the results summarized here, there was a certain controversy about *I* conditions, followed by certain urgency so as to understand the different effect of mono- and divalent cations in the structure of the phospholipid bilayers. Again, it was Böckmann et al. who shed some light on this question, reporting that, while Na^+ is able to coordinate up to 3 carbonyl oxygen atoms in PC phospholipids, Ca^{2+} can coordinate 4 of them and that this coordination increment requires a further phospholipid reorientation and an improved molecular ordering, which results in a noticeable lipid diffusion reduction respect to the Na^+-coordinated bilayer. Sachs et al.[307], in a comprehensive work

dealing with the orientation changes induced in the PC headgroups as a function of different monovalent cations, reported that chaotropic ions[308], that is, those which are more prone to break water structure (e.g. ClO_4^- and I^-), can penetrate more deeply in the polar headgroup and bind more strongly to it. They reported that the ionic population is maximum between the phosphate and the carbonyl groups and that the headgroup tilting is changed independently of the monovalent ion in the medium. The mechanism of this reorientation process is based on electrostatic interactions: the cations push the phosphate group towards the bilayer core, while the anions attract the choline group to the bilayer surface, similarly to the Makino et al. model[301] depicted in Fig. 33.

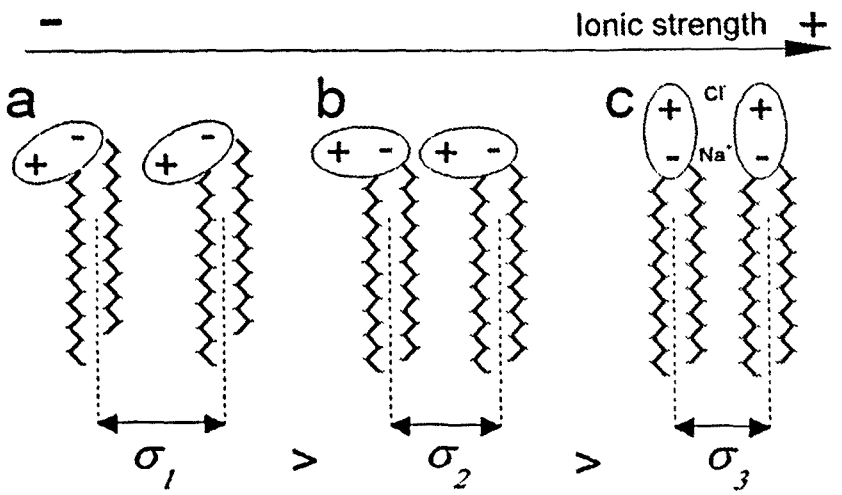

Fig. 33. Phospholipid headgroup tilting induced by ionic strength (model proposed by Makino et al.[301]). a) At low *I* values, the PC headgroups are tilted to maximize electrostatic interactions between phosphate and choline groups. Nevertheless, the distance between adjacent hydrocarbon chains (σ) is far from the optimum van der Waals interaction. b) and c) As *I* increases, the ions place between the headgroup charges and establish robust electrostatic nets, resulting in a membrane thickness increase and, consequently, in a smaller σ. The smaller interchain distance also promotes stronger van der Waals interactions, which contribute to the overall increment of bilayer mechanical resistance.

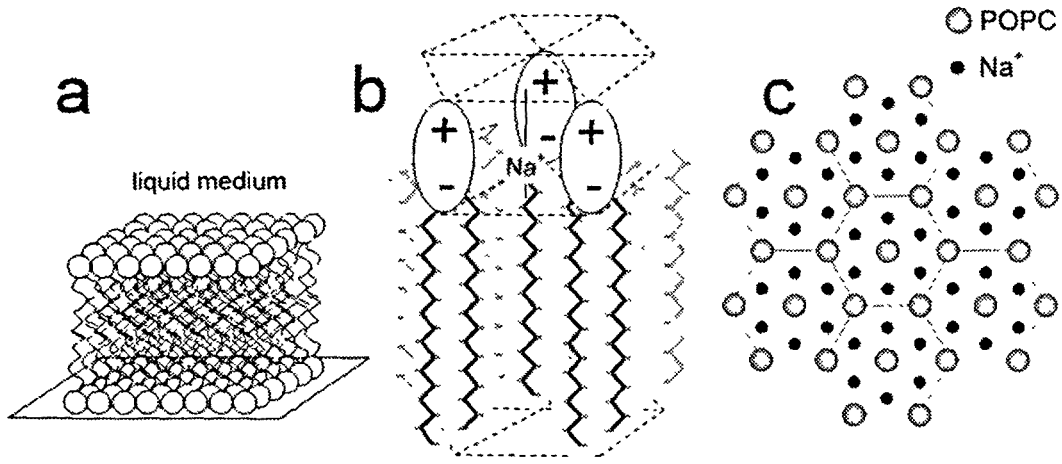

Fig. 34. Insertion of Na^+ cations in the structure of PC membranes proposed by Böckmann et al.[304] a) Phospholipid SPB, where the hexagonal molecular arrangement can be seen. b) Zoom of the upper monolayer where the PC polar moiety is represented by a – (phosphate group) and a + (choline group). At high concentrations of NaCl, each Na^+ cation coordinates with three phospholipid molecules (the coordination number can be 4 for divalent cations as Ca^{2+}) and penetrates the polar moiety up to the phosphate group. c) Upper vision of the same structure.

5.3 PROBING PHOSPHOLIPID BILAYERS WITH AN AFM

5.3.1 Electrostatic double layer forces. Are they enough to explain interactions between tip and sample?

AFM has proved to be a really suitable technique to investigate the properties of a wide range of supported organic structures. Nevertheless, testing the purely mechanical properties of these substances without having any interference in the results becomes a real pain. In the case of Force Spectroscopy in liquid environment, isolating and quantifying electrostatic double layers is one of the most challenging goals that the AFM spectroscopist has to face. Fortunately, there is quite a lot of good quality information about this topic, which will be summarized in this chapter.

To begin with, we should remember that, when deposited on a polar substrate, phospholipid bilayers arranges directing their their polar moieties towards the liquid medium (and to the substrate, of course). No matter whether if

the polar headgroups have net charge or are zwitterionic, they structure the ions in solution forming an electrical double layer[309] that will try to counteract the surface charge. Similarly, AFM tips, both if they are made of Si_3N_4 or SiO_2, have a certain surface charge and, consequently, will also structure ions around them forming an electrical double layer[310]. According to this, a simple model is depicted in Fig. 35, where the charged interface represents the phospholipid bilayer or the AFM tip. As you may expect, when the AFM probe approaches the membrane surface, the electrical double layers interact before undergoing electronic overlapping contact (also called Born repulsion) between the solid surfaces. All these interactions are experimentally detected as a cantilever deflection; the problem is that we can misinterpret the deflection and think that the tip and the sample are in contact, while they are still some nanometers apart, as it is shown in the cartoon depicted in Fig. 36; if the tip and the sample have opposite charge, the tip bends downwards and jumps into contact with the sample due to electrostatic attraction (Fig. 36*a*) and, although the contact point is easily defined, the zero of F_v values becomes somewhat ambiguous in the approaching Δx vs. Δz curve. The opposite case corresponds to a repulsive interaction (Fig. 36*b*) where, despite having a clear F_v reference value (F_v = 0 nN corresponds with the cantilever deflection when the tip is far from the surface), now the contact point is not well defined. Of course, as our goal is to obtain qualitative mechanical information from membranes, it is necessary to understand these electrostatic interactions and separate them from the real sample compression.

A pioneer work by Ishino et al.[311,312] dealt with the effect of electrical charges in Force Spectroscopy experiments, that is, the way the AFM probe deflects as it approaches the sample before touching. Although Ishinos group did not work with phospholipids, the experiments are somewhat revealing and worth mentioning. He demonstrated that similar monolayers only differing in the terminal functional group (stearyl amine or $-CH_3$) interact differently with a Si_3N_4 tip while performing Force Spectroscopy experiments. The zeta-potential measurements for Si_3N_4 surfaces show a point of zero charge around pH 3.0, which means that the tip

is positively charged below this pH and negatively charged above it. Similarly, stearyl amine monolayers have a pKa = 8.5, so they are positively charged below pH 8.5. Then, it is clear that between pH 3.0 and 8.5, tip and monolayer have contrary charges, fact that results in a strong attraction between both bodies that materializes as a strong *jump-to-contact* event. Similar experiments performed on stearic acid monolayers (pH 8.5[313]), showed a similar *jump-to-contact* phenomenon for pH values below 8.5 but a strong repulsion above this value, as it would correspond to two surfaces negatively charged. It is interesting to grasp this repulsion concept in a nanometric way; in the absence of electrostatic interactions, we know that the AFM tip is touching the sample surface because the cantilever bends upwards, although we can not assure a true contact if there is electrostatic repulsion. This effect was used by Senden et al.[252] to develop a new AFM operation mode (Electrical Double Layer mode). The authors claimed that any repulsive interaction is, in principle, eager to be used as a feedback signal to obtain topographic AFM images. Besides, the long range nature of electrostatic forces makes of them a suitable feedback signal for nondestructive imaging strategies. They imaged a Si_3N_4 sample with an AFM tip made of the same material, observing that when both surfaces are clearly negative and the Δx vs. Δz curves show repulsion between them, it is possible to obtain an AFM image in the non-contact region.

Interestingly, the tip-sample distance in this Electrical Double Layer mode can be modulated changing the electrolyte concentration in the medium as established by Debye:

$$\lambda_D = \sqrt{\frac{\varepsilon_0 \varepsilon_r k_b T}{2 N_A e^2 I}} \tag{30}$$

Where λ_D is the Debye length and ε_r is the dielectric constant. λ_D value is considered as the thickness of the electrical double layer, a really important parameter to modulate the tip-sample distance and kind of interaction. In this direction, Müller et al.[314] proposed that finely tuned I and pH conditions are

necessary to obtain high resolution AFM images of soft biomolecules, which are delicate and easily altered by the pressure exerted by the AFM tip while scanning. Adjusting these parameters, the optimum repulsive interaction regime, which consists on a strong electrostatic repulsion with a short λ_D, can be obtained.

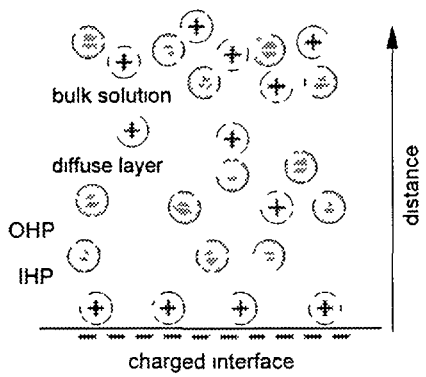

Fig. 35. Charged interface in contact with an electrolyte and formation of the electrical double layer. The surface charge structures the ions in the form of an Internal Helmholtz plane (IHP), outer Helmholtz plane (UHP) and diffuse layer. For higher distances from the charged interface, the ions do not feel the presence of the sample charge.

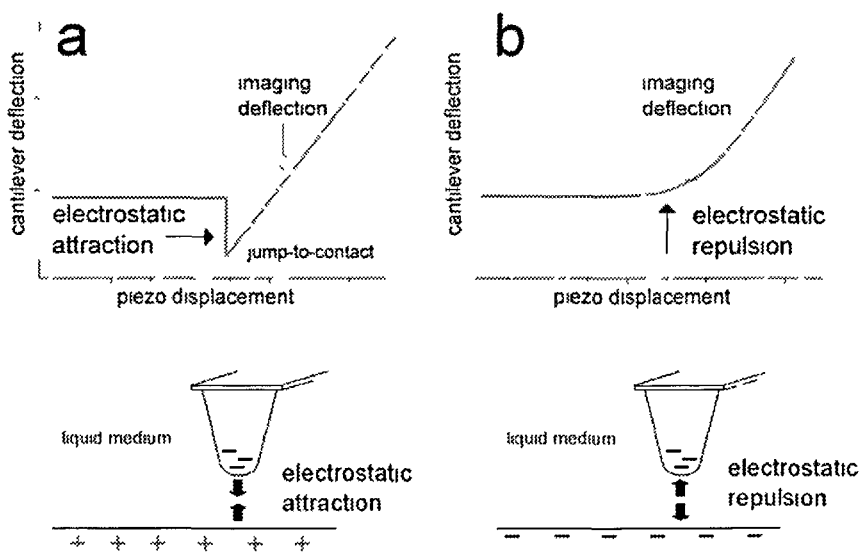

Fig. 36. Electrostatic interactions between sample and tip. a) Attractive interaction, which is seen as a strong *jump-to-contact* event in the approaching Δx *vs.* Δz curve. In this case, topographic image has to be acquired in a Born contact basis (repulsion due to electron overlapping). b) Repulsive interaction, which is detected by a cantilever deflection before Born contact. Imaging can be done in a non-contact regime (Electrical Double Layer mode proposed by Senden et al.[310]). The double-layer has been omitted in the representations for the sake of simplicity. The dotted line represents the deflection at which images are acquired or setpoint cantilever deflection.

5.3.1.1 DLVO theory: unifying electrostatic and van der Waals interactions in the nano- range.

In order to understand the interactions between tip and sample we must be aware of the dimensions of the surfaces in contact. As a starting point, gravitational forces are not dominant at this range but forces acting in a radius of action below 100 nm must be considered[315]. These interactions, mainly electrostatic and van der Waals forces, are electromagnetic in nature and were unified in the so-named DLVO theory proposed by Derjaguin and Landau[316] and refined by Verwey and Overbeek[317], providing a comprehensive basis for studying surface interactions.

The basis of van der Waals forces is the dipolar correlation between the contacting surfaces. These interactions are time dependent, as they can be due to orientation changes in permanent dipoles or to dipoles that modify their charge with time, being this second possibility, known as dispersion interaction, the one that usually dominates van der Waals forces. These interactions, despite being present in all surfaces as all atoms are polarizable in some extent, are extremely short ranged (they are proportional to D^{-7}, being D the separation between the tip and the sample) and mostly weakly attractive.

As a first approximation, the van der Waals forces between a plane and a sphere of radius R are given by

$$F_{vdW} = -\frac{HR}{6D^2} \tag{31}$$

where H stands for the Hamaker constant[59,277,318,319], which depends on the dielectric constant of the contacting surfaces and the medium they are immersed in.

The electrostatic interaction between a charged sphere and a charged plane can be written as[315,320,321]

$$F_{el} = \frac{4\pi R\delta_1\delta_2\lambda_D}{\varepsilon_r\varepsilon_0} \times e^{-\frac{D}{\lambda_D}} \tag{32}$$

Where δ_1 and δ_2 are the surface charge densities of the tip and the sample. Finally,

$$F_{DLVO} = F_{vdW} + F_{el} \tag{33}$$

5.3.1.2 What happens when a phospholipid bilayer is compressed? Classical mechanics meets DLVO theory.

I guess this is a good point to gather all the interactions that have been reviewed until this point. We have seen that phospholipid bilayers structure highly depends on the ions that are present in the solution and on the pH. These two parameters are crucial because they change the interactions between polar heads, creating ionic networks between phospholipid molecules and electrolytes that increase the molecular packing, changing the orientation of the polar heads due to electrostatic repulsions and also modifying the van der Waals interactions between the hydrocarbon chains, highly dependent on the intermolecular distance. The pH conditions can result in a protonation or deprotonation of the phospholipid polar moieties, dramatically changing the electrostatic equilibrium between individual phospholipid molecules and also between the bilayer and the substrate. Besides, we have seen that electrolyte double layers are formed on top of the bilayer as a consequence of the polar headgroups charge separation (in the case of neutral polar groups) or due to the presence of net charge (in charged headgroups). Of course, as the AFM tip is also charged, the double layers of the two surfaces overlap and extra forces arise. Fortunately, DLVO theory provides a comprehensive way to quantify the van der Waals and electrostatic interactions between the tip and the membrane but, as the tip compresses the bilayer, both the DLVO forces and the bilayer mechanical resistance are probed at the same time. Can both contributions be separated? Can the mechanical process of membrane compression be understood? Can meaningful and quantitative mechanical parameters be extracted?

Firstly, we should revise the work by Schneider et al.[322], where they prepared LB phospholipid bilayers and explored the effect of the polar heads and

the hydrocarbon chain unsaturations in the mechanical properties of the bilayers. They performed the measurements in pure water to avoid the formation of electrolyte double layers, which is a good starting point despite not being really meaningful in a strict physiological sense, and coated the tip with a –OH terminated thiol so as to control the tip charge and its chemistry[323] (Fig. 37). They observed that, when the bilayer is compressed, a sudden jump in the F_v vs. P_d curves appears when a threshold F_v value is reached. This jump was identified as a sudden bilayer puncturing, phenomenon that had been previously observed in SFA experiments on similar samples[324,325] and on fatty acid layers[326]. Schneider et al. found that if the F_v value at which the breakthrough event takes place (F_y) is divided by the tip R, then F_y value becomes reproducible and has a different value for each of the three tested phospholipids, pointing out that structural differences can be sensed by means of breakthrough events detection and quantification. It is interesting to highlight that dividing by the tip R, the authors attempted to normalize all the measurements, which were practically performed with different tips. Apparently, the higher the R, the higher the A value and the higher the F_v that must be applied on the monolayer to break it, as the pressure applied on the monolayer is the real figure of merit. Nevertheless, this would work if the entire tip apex was in contact with the sample; in fact this is the never-ending *real A - apparent A* controversy, where frictional measurements that prove why *real* and *apparent A* are not always proportional are discussed.

Franz et al.[70] studied the breakthrough event in more detail, concluding that F_y value increases with tip penetration velocity. It was also revealed that the penetration magnitude (the total height change during the breakthrough event) decreases in magnitude when tip velocity increases, fact that was attributed to the elastic-plastic properties of the bilayer; as the tip compresses the bilayer more rapidly, the membrane is deformed up to a higher extent before being punctured, which results in a thinner bilayer prior to the rupture process. This fact is consistent with the F_y value increment with tip velocity, as higher F_y values would result in higher bilayer deformation. A F_v vs. P_d curve is depicted in Fig. 38, where the

different regions concerning the elastic sample deformation prior to the bilayer rupture and the sudden penetration event are depicted. Franz also detected the presence of double jumps corresponding to the puncturing of two bilayers only when using high *R* tips. They proposed that expulsed phospholipid molecules are more prone to form a bilayer on high R tips (>90 nm), as in these conditions the tip apex is like a flat surface if compared with the dimensions of a phospholipid bilayer. Then, phospholipid molecules expulsed after puncturing would form a bilayer on the tip, so the two detected breakthrough events in posterior nanoindentation experiments would correspond to the disruption of the tip bilayer and the sample bilayer. This hypothesis was supported by posterior experiments with functionalized tips, where the spontaneous formation of bilayers on the tip surface was not detected for small tip *R* values[327]. They also found that is possible to observe breakthrough events both in liquid and solid phases, which had been a matter of debate during the last years[322,328].

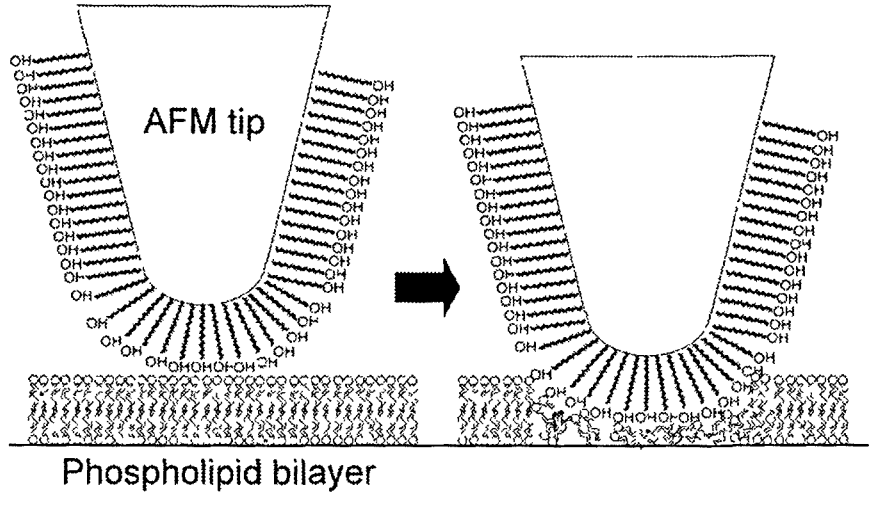

Fig. 37. Model of phospholipid bilayer breakthrough proposed by Schneider et al.[322] In order to control the chemistry of the tip, it is coated with alkanethiols. The Δx vs. Δz curves render reproducible F_y values.

Force Spectroscopy experiments also helped to understand in more detail the membrane fusion process. As we have seen, a threshold F_y value is necessary to penetrate a bilayer but in membrane fusion processes it is not likely that this energy is available. Then, how does the membrane fusion works? Schneider et al.[329] shed

some light on this issue, performing Δx *vs.* Δz curves on a variety of phospholipid bilayers with tips functionalized with –OH terminated and $-CH_3$ terminated alkyl chains. They observed variations in F_y value for several phospholipid bilayers when using –OH terminated tips but, strikingly, F_y was near 0 when $-CH_3$ terminated tips were used. In all these experiments electrostatic forces were minimized (no electrolyte, no double-layer interactions), so the F_y values obtained for hydrophilic tips (-OH terminated) were attributed to the intrinsic mechanical bilayer resistance and to hydration forces, both detected as a steep repulsion in the contact between tip and sample. Using a hydrophobic tip minimized the hydration forces, fact that was experimentally verified as a lack of repulsion in the contact region, and a F_y value reduction was expected. Nevertheless, there was a certain attraction between the two surfaces, which was attributed to an interdigitation between the tip hydrocarbon chains and the bilayer core. This hypothesis leans on previous results presented by Schneider et al.[322], who claimed that as the tip compresses the bilayer and reaches its elastic limit, some defects are generated on the phospholipid structure, acting as bilayer rupture nucleation points.

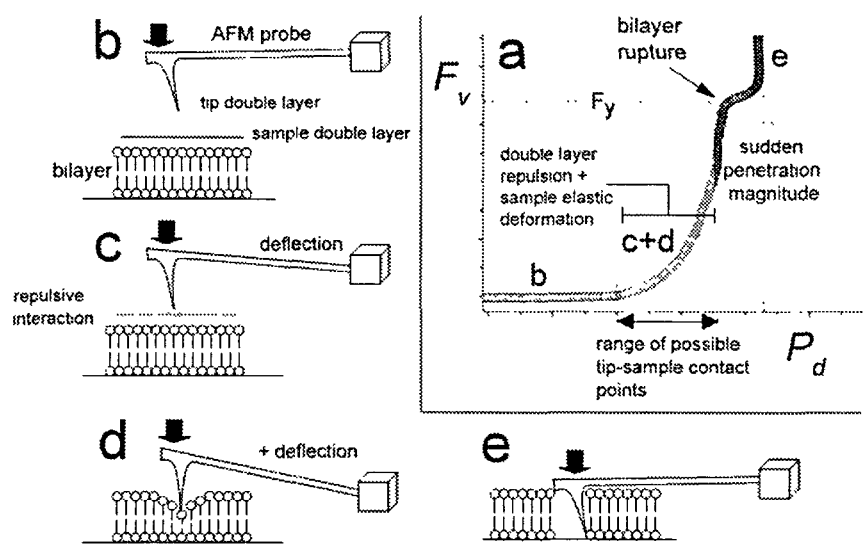

Fig. 38. a) F_v vs. P_d curve performed on a phospholipid bilayer in liquid environment. b) The tip is far from the surface and the double layers of tip and sample do not interact, so $\Delta x \sim 0$. c) Assuming that the tip and the sample are both charged negatively, the interaction between the double layers results in an electrostatic repulsion, which is experimentally detected as a Δx. d) The tip contacts the bilayer and deforms its structure. Note that b) and c) cannot be discerned in the F_v vs. P_d curve shown in a), as both the electrostatic repulsion

and the bilayer mechanical resistance are detected as a Δx increment. e) Bilayer rupture at $F_v = F_y$.

A further step was taken by Pera et al.[327] who studied the interaction between different phospholipid bilayers by means of Force Spectroscopy. To do that, they functionalized the AFM tips with hydroxy-terminated alkanethiols, which were proved to be a suitable substrate for the deposition of phospholipid liposomes obtaining, for the first time, stable phospholipid bilayers on an AFM tip apex. This work presents really interesting results: when a Δx vs. Δz curve is performed on a clean mica surface with a hydroxy- terminated tip, a breakthrough event in the F_v vs. P_d curve is detected, demonstrating the quality of the deposited bilayer and the nature of the rupture event in spectroscopy experiments. We must remember that until then there was not a really clear prove that the sudden jump in the Δx vs. Δz curve corresponded with the film breakthrough although after remarkable works by Dûfrene[330], Schneider[322,329], Butt[68], Tiberg[331], Richter[332] and Künneke[71] it seemed quite an obvious explanation. Two possible mechanisms were proposed for the double penetration events detected in Δx vs. Δz curves when using tips coated with phospholipid bilayers, as it is depicted in Fig. 39; the first one corresponds with the simultaneous rupture of the monolayers in contact with the liquid medium forming a single bilayer followed by the consequent rupture of this bilayer, while the second one corresponds with the consecutive rupture of the individual bilayers present in the interface. Interestingly, and according to the different interaction energy between phospholipid molecules and mica or hidroxy- terminated alkanethiols, the F_y value for tip-adsorbed bilayers is noticeably lower than that for bilayers adsorbed on the mica surface[68]. Finally, and according to previously published experiments, a breakthrough event was detected when performing Δx vs. Δz curves on a mica supported bilayer with an uncoated tip. As it is common knowledge, high-quality, meaningful experiments always pose new questions and reopen old debates and Pera's work was not an exception: When testing a certain sample with a certain tip, they confirmed that F_y values dispersion was really small but when changing the tip or the sample for an "identical" one, great variations were recorded. These differences were attributed to several factors; To begin with, the tip

shape can influence the results (do you remember all the discussions about the *apparent* and the *real A* value and the different contact mechanics models proposed?), although a clear relationship between F_y value and the tip R was not obtained, fact that was in clear contradiction with the works by Schneider et al.[322,329]. It was also proposed that the molecules that functionalize the tip can be removed while performing Δx vs. Δz curves, which in fact is a plausible hypothesis because the pressures applied on the tip apex can reach the GPa regime[333].

Interestingly, Pera et al. detected that Δx vs. Δz curves between two bilayers always yielded a repulsive interaction in the contact region; as DLVO forces comprise van der Waals (attractive) and electrostatic interactions (repulsive when the composition of the bilayers is the same), the authors concluded that electrostatic forces are dominant in the contact region. In fact, the van der Waals interaction for a tip with a R = 100 nm is 50pN for a D = 1 nm[334]. They further investigated the nature of the contact region changing I magnitude. As expressed in equation 30, if I value is decreased, λ_D increases and the electrostatic repulsive interaction between double layers extend over a longer distance, being detected as a Δx variation up to 30 nm far from the sample surface. Besides, the double jump when Δx vs. Δz curves between functionalized tips and mica supported bilayers are not observed (just the breakthrough event corresponding with the mica supported bilayer is detected), demonstrating that tip-supported bilayers are weakly adsorbed and that are highly dependent on the electrolyte concentration.

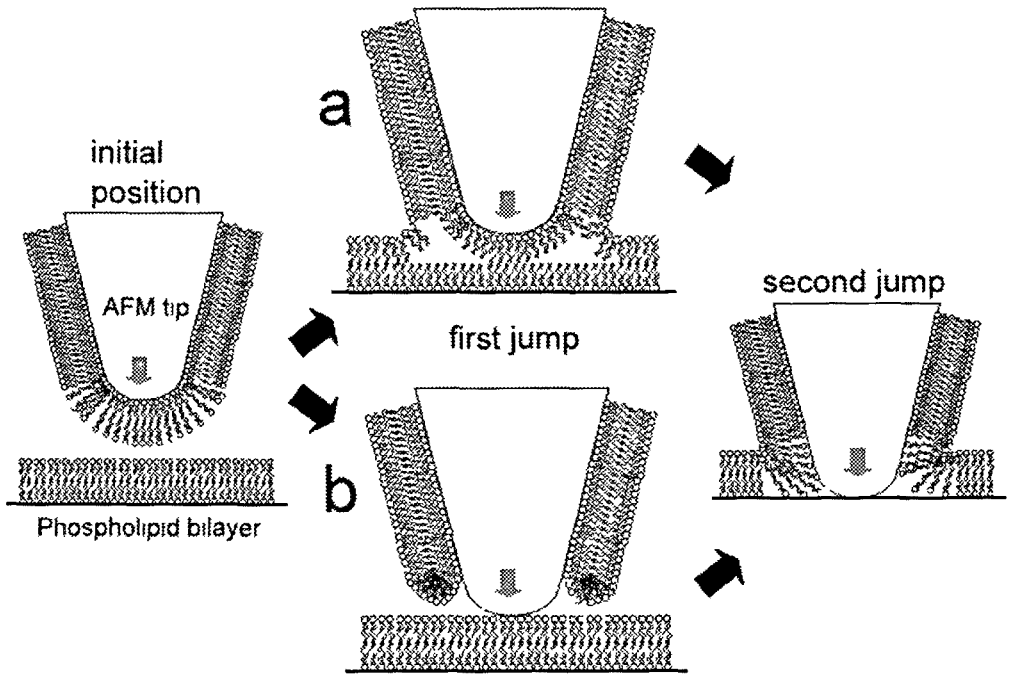

Fig. 39. Δx vs. Δz curves performed on a mica supported phospholipid bilayer with an equally functionalized tip (the tip is coated with gold and a hidroxy- terminated alkanethiol monolayer to improve the adherence of the phospholipid bilayer). Two individual breakthrough events are detected and Pera et al.[327] proposed two different mechanisms. a) Rupture of the outer monolayers both in tip and sample to form a bilayer or b) rupture of the tip bilayer, which proves to be less mechanically robust. The second jump leads to the rupture of the phospholipid structures and to the consequent hard-contact between the tip and the mica surface.

5.3.2 Effect of pH. Chemical Force Microscopy - A novel method to probe surface interactions

In this section, I would like to introduce the Chemical Force Microscopy[196,248,335,336] as a powerful technique to detect and quantify molecular interactions at the nanometric level. In fact, it is based on the F_A experimental measurement between an AFM probe (that can be functionalized to meet specific requirements) and the sample of study. F_A value, which is calculated as the lowest point in the retraction Δx vs. Δz curve minus the baseline (Fig. 18), responds to the different attractive and repulsive interactions that arise between the tip and the sample as they come into contact. This technique has been widely used to test different functional groups in different pH conditions, so I will begin with a brief

review of experimental soultions proposed in the past. After that, I will comment on the only Chemical Force Microscopy work performed on phospholipid bilayers that has been able to sense the changes that bilayers undergo at different pH values. Besides, it is worth mentioning that this work was performed in our lab and, although several techniques have been used in the past to assess the effect of pH on phospholipid bilayers, this is, to the best of our knowledge, the only contribution to the topic were nanometric measurements are involved.

I find quite didactic to comment on the work released by Vezenov et al.[337] concerning Chemical Force Microscopy, as it is exhaustive and comprehensive. After functionalizing both Si_3N_4 tips and gold coated substrates with NH_2/NH_3^+ terminated SAMs, they performed Δx vs. Δz curves, finding that F_A value is practically 0 below pH 4 while it increases in a sigmoidal way to reach a plateau around pH 6 (Fig. 40*a*). It is important to note that F_A changes can be due both to the mechanical properties of the interacting monolayers and to the different van der Waals, steric, hydration and electrostatic forces altered by the change in pH. Nevertheless, in these experiments the mechanical contribution was eliminated because the only changes were introduced in the ionization state of the terminal groups. With this in mind and considering that F_A changes were only due to the different electrostatic interactions between terminal groups and AFM tip, the authors considered that the pKa of the amine groups in the monolayers was around 4. Consequently, below pH 4, both the tip and the sample surface are positively charged and the electrostatic repulsion is responsible for the extremely low F_A value. At pH values higher than 4, the amine groups deprotonate and the electrostatic repulsion disappears, while van der Waals interactions become dominant. Interestingly, the pKa of amines in solution is 10-11, so a remarkable pKa shift is seen between amines in solution and monolayers[337]. This is an interesting point, where it is quite clear that our classical chemical knowledge must be revisited when the reactions are considered from a nanometric point of view. This effect has been detected in previous works[338-340] and attributed to the surface molecules number of freedom degrees reduction, changes in the dielectric constant

of the solution[341] and different terminal groups solvation degree. The same kind of measurements were performed with –COOH functionalized surfaces obtaining an F_A change around pH 5.5 (fig. 40*b*). Nevertheless, this time F_A was high at low pH values while it decreased to a steady plateau around 0nN for high pH values. Obviously, the high F_A values are due to the formation of hydrogen bonds between the protonated carboxylic acid groups while the low F_A values were attributed to electrostatic repulsion between $-COO^-$ groups.

Friction measurements can also be used to assess the interaction forces between surfaces. For –COOH terminated tips and samples, F_f vs. F_v curves demonstrated that F_f is always higher than for $-COO^-$ terminated interfaces. In fact, friction measurements complement Force Spectroscopy experiments, as it is another way to quantify interactions between surfaces. Then, when groups that are negatively charges are rubbed together, electrostatic repulsion prevents the two surfaces from interacting, which results in low F_f values. On the other hand, the protonated carboxylic groups form hydrogen bonds while they are in contact and this effect leads to a F_f value increment. Similarly, μ is also sensitive to the pH value and the obtained experimental μ vs. pH curves are very similar to the A_d vs. pH ones. To conclude, and just in case someone had any doubt about the protonation/deprotonation process being responsible for the observed experimental changes, they functionalized the interfaces with –OH terminated SAMs and, as you would expect, both friction coefficient and adhesion forces proved to be independent from the pH as the –OH groups cannot be deprotonated between pH 2 and 12. How elegant, don't you think?

Now that we have some notions about the Chemical Force Microscopy capabilities, it is time to apply it to PC bilayers. The electrostatic interactions present in these membranes are due to the polar headgroups which, despite being neutral, show charge separation. Besides, there is one ionizable group in the phosphate moiety, so the head has a certain pKa. Phospholipid pKa can be experimentally measured by several techniques as surface potential measurements[342] or classical titrations[343], although these techniques only work for

liposomes in solution and not for supported layers and we have seen before that pKa values can change a lot depending on the structural disposition of the molecules[338-341,344]. according to this, Garcia-Manyes et al.[345] performed Δx vs. Δz curves on DMPC and 1,2-Dilauroyl-*sn*-Glycero-3-Phosphocholine (DLPC) bilayers with –COOH terminated AFM tips and studied the approaching curves instead of the retraction ones with the object of avoiding any extra interactions because of bilayer damage.

This is the point to gather some of our knowledge about phospholipid bilayers and the electrostatic interactions that affect them, as the experiments reported by Garcia-Manyes et al. combine some of these concepts in a very fruitful way. PC bilayers have a residual negative charge in pure water that can be modulated[298] (and sign reversed) increasing I value. Zeta-potential experiments show that the 0 charge point for DMPC is obtained at 100 mM NaCl at neutral pH